ผลของโปรโมเตอร์ต่อสมบัติของตัวเร่งปฏิกิริยาโคบอลต์บนแกมมาอลูมินาเตรียมโดยปฏิกิริยาในสถานะของแข็งสำหรับปฏิกิริยาคาร์บอนไดออกไซด์ไฮโดรจิเนชัน

นางสาวมินตรา สังข์สุข

วิทยานิพนธ์นี้เป็นส่วนหนึ่งของการศึกษาตามหลักสูตรปริญญาวิศวกรรมศาสตรมหาบัณฑิต
สาขาวิชาวิศวกรรมเคมี ภาควิชาวิศวกรรมเคมี
คณะวิศวกรรมศาสตร์ จุฬาลงกรณ์มหาวิทยาลัย
ปีการศึกษา 2556

EFFECT OF PROMOTERS ON THE PROPERTIES OF Co/γ-Al2O3 CATALYSTS PREPARED BY SOLID-STATE REACTION FOR CO2 HYDROGENATION

Miss Mintra Sungsook

A Thesis Submitted in Partial Fulfillment of the Requirements
for the Degree of Master of Engineering Program in Chemical Engineering
Department of Chemical Engineering
Faculty of Engineering
Chulalongkorn University
Academic Year 2013

Thesis Title	EFFECT OF PROMOTERS ON THE PROPERTIES OF Co/γ-Al2O3 CATALYSTS PREPARED BY SOLID-STATE REACTION FOR CO2 HYDROGENATION
By	Miss Mintra Sungsook
Field of Study	Chemical Engineering
Thesis Advisor	Associate Professor Joongjai Panpranot, Ph.D.

Accepted by the Faculty of Engineering, Chulalongkorn University in Partial Fulfillment of the Requirements for the Master's Degree

.....Dean of the Faculty of Engineering

(Professor Bundhit Eua-arporn, Ph.D.)

THESIS COMMITTEE

.....Chairman

(Associate Professor Muenduen Phisalaphong, Ph.D.)

.....Thesis Advisor

(Associate Professor Joongjai Panpranot, Ph.D.)

.....Examiner

(Associate Professor Anongnat Somwangthanaroj, Ph.D.)

.....External Examiner

(Assistant Professor Okorn Mekasuwandumrong, D.Eng.)

มินตรา สังข์สุข : ผลของโปรโมเตอร์ต่อสมบัติของตัวเร่งปฏิกิริยาโคบอลต์บนแกมมาอลูมินาเตรียมโดยปฏิกิริยาในสถานะของแข็งสำหรับปฏิกิริยาคาร์บอนไดออกไซด์ไฮโดรจิเนชัน. (EFFECT OF PROMOTERS ON THE PROPERTIES OF Co/γ-Al2O3 CATALYSTS PREPARED BY SOLID-STATE REACTION FOR CO2 HYDROGENATION) อ.ที่ปรึกษาวิทยานิพนธ์หลัก: รศ. ดร. จูงใจ ปั้นประณต, 108 หน้า.

ศึกษาผลของการเติมโปรโมเตอร์ ได้แก่ โพแทสเซียม แมงกานีส คอปเปอร์ และซีเรียม บนตัวเร่งปฏิกิริยาโคบอลต์บนอลูมินาที่เตรียมด้วยปฏิกิริยาในสถานะของแข็งและวิธีการเคลือบฝัง ทำการตรวจพิสูจน์เอกลักษณ์ของตัวเร่งปฏิกิริยาด้วยเทคนิควิเคราะห์ที่หลากหลาย เช่น การเลี้ยวเบนของรังสีเอกซ์ เอกซเรย์โฟโตอิเล็กตรอนสเปกโตรสโคปี วัดพื้นที่ผิว การรีดักชันแบบโปรแกรมอุณหภูมิสูง กล้องจุลทรรศอิเล็กตรอนแบบส่องกราดและการดูดซับทางเคมีด้วยไฮโดรเจน ทดสอบประสิทธิภาพของตัวเร่งปฏิกิริยาในปฏิกิริยาคาร์บอนไดออกไซด์ไฮโดรจิเนชันที่ความดัน 1 บรรยากาศและอุณหภูมิ 270 องศาเซลเซียสในเครื่องปฏิกรณ์แบบเบดนิ่ง พบว่าค่าการแปลงผันของคาร์บอนไดออกไซด์เพิ่มขึ้นเมื่อมีการเติมโดยเรียงลำดับดังนี้ 1KCo > 1MnCo > 1CeCo > Co >1CuCo สำหรับตัวเร่งปฏิกิริยาที่เติมโปรโมเตอร์ร้อยละ 1 โดยน้ำหนัก ตัวเร่งปฏิกิริยที่เติมโปรโมเตอร์ทุกตัวให้ค่าการเลือกเกิดของมีเทนเป็น 100 เปอร์เซ็นต์ การเติมโปรโมเตอร์บนตัวเร่งปฏิกิริยาโคบอลต์บนอลูมินาส่งผลต่อการเพิ่มพื้นผิวและปริมาณรูพรุนซึ่งส่งผลให้ค่าของการกระจายตัวของโคบอลต์เพิ่มขึ้น สำหรับตัวเร่งปฏิกิริยาโคบอลต์บนอลูมินาที่เตรียมด้วยปริมาณของโพแทสเซียมและแมงกานีสในช่วงร้อยละ 0.5-2.0 โดยมวลด้วยปฏิกิริยาในสถานะของแข็งและวิธีการฝังตัว ผลสุดท้ายพบว่าตัวเร่งปฏิกิริยาที่เติมโปรโมเตอร์ร้อยละ 1 โดยน้ำหนักมีความเหมาะสมที่สุดสำหรับปฏิกิริยาคาร์บอนไดออกไซด์ไฮโดรจิเนชัน การเติมปริมาณของโปรโมเตอร์ที่มากเกินไปที่ร้อยละ 2 โดยน้ำหนักส่งผลพื้นผิวที่ว่องไวบนตัวเร่งปฏิกิริยาลดลงและลดการเกิดมีเทนซึ่งเป็นผลิตภัณฑ์หลักที่ต้องการ

ภาควิชา	วิศวกรรมเคมี	ลายมือชื่อนิสิต .....
สาขาวิชา	วิศวกรรมเคมี	ลายมือชื่อ อ.ที่ปรึกษาวิทยานิพนธ์หลัก .....
ปีการศึกษา	2556	

5570336221 : MAJOR CHEMICAL ENGINEERING
KEYWORDS: CO2 HYDROGENATION / PROMOTER / COBALT CATALYST / SOLID-STATE REACTION

MINTRA SUNGSOOK: EFFECT OF PROMOTERS ON THE PROPERTIES OF CO/Y-AL2O3 CATALYSTS PREPARED BY SOLID-STATE REACTION FOR CO2 HYDROGENATION. ADVISOR: ASSOC. PROF. JOONGJAI PANPRANOT, Ph.D., 108 pp.

The addition of different promoters (K, Mn, Cu, or Ce) over Co/□-Al2O3 catalysts was investigated. The catalysts were prepared by solid-state reaction and incipient wetness impregnation (IWI) method. The catalysts were characterized by various methods such as XRD, XPS, BET, ICP, TPR, SEM, and H2-chemisorption. Their catalytic performances were evaluated in the CO2 hydrogenation at atmospheric pressure and 270 °C in a fixed-bed reactor. The results show that under the reaction conditions, the addition of promoters increased the CO2 conversion in the order: 1KCo > 1MnCo > 1CeCo > Co > 1CuCo for 1 wt.% promoters loading. All the promoted catalysts exhibited 100% CH4 selectivity. The addition of promoters over Co/□-Al2O3 bring about the higher catalyst surface area and pore volume leading to higher Co dispersion and higher reducibility of Co3O4 crystallites. A series of Co/□-Al2O3 catalysts were also prepared with various amounts of K and Mn loading ranging from 0.5 to 2.0 wt.% by solid-state reaction and incipient wetness impregnation method. Conclusively, the addition of 1 wt.% of K and Mn was found to be appropriate for the CO2 hydrogenation. Excessive amount of promoter at 2 wt.% led to lower amount of the active metal and as a consequence the CH4 formation which was the desired product was decreased.

Department:	Chemical Engineering	Student's Signature	.....
Field of Study:	Chemical Engineering	Advisor's Signature	.....
Academic Year:	2013		

ACKNOWLEDGEMENTS

First and foremost, I would like to express my deepest and sincerest gratefulness to my adviser, Associate Professor Dr. Joongjai Panpranot for her kindness in providing an opportunity and precious time to her advisee. I am also extremely appreciated and indebted for her expertise, sincere and valuable supervision, suggestion, supporting, guidance and encouragement to me throughout my research.

I also place on record, my sense of gratitude to all who, directly or indirectly, have lent their helping hand and various suggestions in this venture.

CONTENTS

Page

Page

Page

LIST OF TABLES

Page

Page

LIST OF FIGURES

Page

Page

CHAPTER I

INTRODUCTION

1.1 General introduction

In the last decades, the concentration of CO_2 into the atmosphere was drastically increased, which led to global warming and climate change. The major sources of energy such as oil, natural gas, and coal were rapidly decreased. Accordingly, scientists have continued to develop efficient CO_2 capture and utilization system. The CO_2 hydrogenation reaction is interested as an effective route for the production of synthetic natural gas (SNG) that has been required during the few last years. This role can improve the security of energy supply and reduce the emission of CO_2 [1].

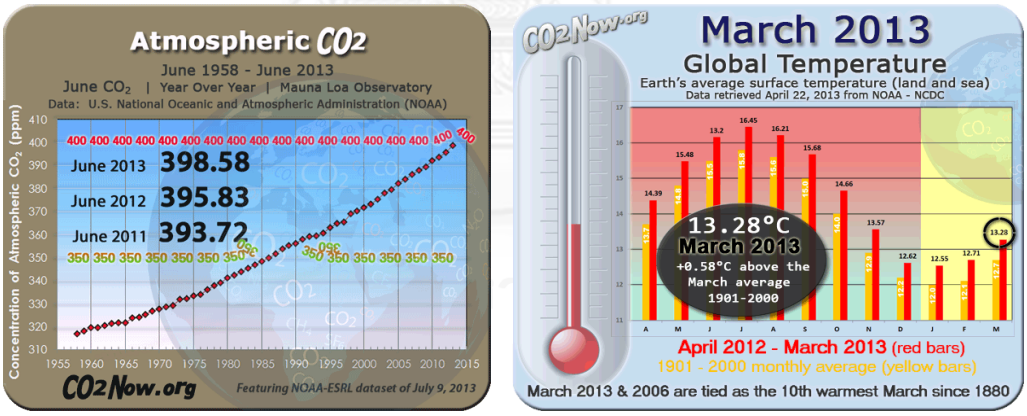

Figure 1.1 Changes in CO_2 emission and average surface temperature [2].

The carbon dioxide hydrogenation ($CO_2 + H_2 \leftrightarrow CH_4 + H_2O$) has been studied by using various catalytic systems composing mostly group VIIIB metals (e.g., Co, Fe, Ni, Ru and Rh) supported on different metal oxides (e.g. SiO_2, TiO2, Al_2O_3, ZrO_2, and CeO_2) [3,4,5,7,8]. Cobalt is the most extensively used catalyst

because of its high resistance to deactivation, lower cost compared to noble metal, high activity, high selectivity for liner hydrocarbon, and low activity for water gas shift (WGS) reaction. The interaction of cobalt with the support has been studied and observed that the factors of the interactions are preparation method [6,7], reduction temperature [3], metal loading [3], catalyst components [4,5,6], and the supports [3]. For instance, among alumina, silica, and magnesia, which have been investigated for synthesis of cobalt catalysts, alumina supported cobalt catalysts resulted in the formation of cobalt aluminate at calcination temperature greater than 973 K and possessed the highest methane yield compared to those supported on silica and magnesia [3]. Alumina is one of supports which are frequently used for preparation of cobalt catalysts. Alumina is a very attractive material for use as catalyst support due to their high surface area, high mechanical resistance, high chemical stability, good catalytic activity, and good thermal stability. However, it has several transition phases such as the eta (η), theta (θ), kappa (κ), chi (χ), delta (δ), and gamma (γ) alumina. The phase transformation of alumina is demonstrated in the Figure 1.2 by beginning from gibbsite ($Al(OH)_3$). The path of transformation depends on various factors such as heating rate, temperature, pressure, and initial raw material [9]. Currently, γ-Al_2O_3 is the most well-known structure that has been used as a support for metal catalyst. Moreover, it has a variety of applications because of its characteristic mechanical, chemical, thermal properties, and high surface area [10].

Cobalt catalysts supported on alumina are important catalyst systems widely used in various reactions such as hydrogenation, stream reforming, and hydrotreating [8]. The interaction between the metal and the support considerably affects the properties of the catalyst. In general, a weaker interaction gives larger

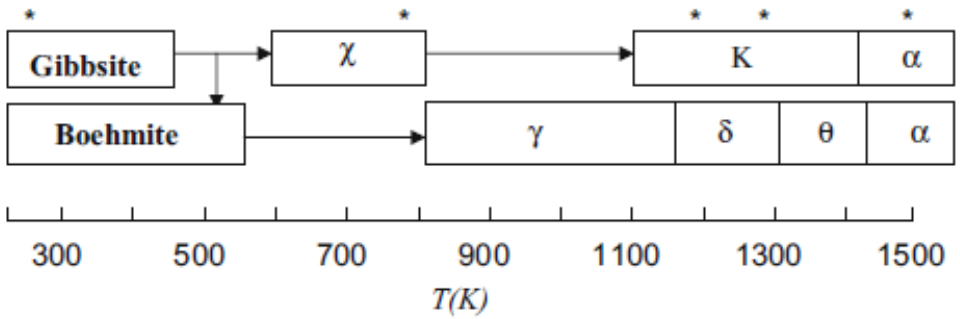

Figure 1.2 Sequence of dehydration and transformation of alumina from gibbsite and boehmite [11].

particles and a higher reducibility whereas a stronger interaction leads to smaller particles and lower reducibility [12]. The metal-support interaction depends on both the support and the catalyst components. The Co/Al_2O_3 catalyst has a limited reducibility because of a strong interaction between the support and the cobalt oxides [13]. The addition of small amount of metals on cobalt catalyst has been aimed in order to increase the reduction degree and the catalytic activity of cobalt catalysts [12]. Improvement of catalyst activity can be achieved by addition of a second metal as promoter that is stable under reaction conditions.

In general, catalyst can be prepared by different methods such as impregnation, spray reaction, microemulsion, and solid-state reaction. The solid-state reaction is extensively used to produce ceramic. The factors which affect to rate of a solid state reaction include surface area and structure properties of the solids and reaction conditions. There are three main benefits for the solid-state reaction. They (i) are simple, cheaper and convenient; (ii) use less solvent and contamination; and (iii) give high yield of product [14].

This research will focus on the effects of type of second metal (K, Mn, Cu, Ce) and amount of second metal loading (0, 0.5, 1.0, 2.0 wt%) on the Co/γ-Al_2O_3 (15% loading Co) catalysts prepared by solid-state reaction. The catalysts will be characterized by X-ray diffractrometer (XRD), X-ray photoelectron spectroscopy (XPS), temperature-programmed reduction (TPR), N_2 physisorption, scanning electron microscope (SEM), and Hydrogen chemisorption. The catalytic activities of the catalysts will be evaluated in the CO_2 hydrogenation reaction under atmospheric pressure.

1.2 Research objective

The objective of this research is to prepare γ-Al_2O_3 supported cobalt catalysts by the solid-state reaction of gibbsite and cobalt precursor with different promoters including K, Mn, Cu, and Ce and investigate their catalytic properties in the carbon dioxide hydrogenation.

1.3 Benefits of the research

This research will improve the catalyst used in CO_2 hydrogenation reaction.

1.4 Research scopes

1.4.1 Preparation of Co/γ-Al_2O_3 and the addition of promoters (K, Mn, Cu, Ce) with Co/γ-Al_2O_3 catalysts by solid-state reaction with gibbsite and calcined at 650 °C

1.4.2 Investigation catalytic activity of the hydrogenation of CO_2 at atmospheric pressure, temperature 270°C, and H_2/CO_2 ratio equal to 10 in a fixed-bed reactor.

1.4.3 Selected the best of promoter which give the highest CO_2 conversion. Investigated the effect of difference amounts of the selected promoter (0.5, 1.0, and 2.0 %wt) on the properties of Co/γ-Al_2O_3.

1.4.4 Characterization of addition of promoters with Co/ γ-Al_2O_3 catalysts and support by using X-ray diffractrometer (XRD), X-ray photoelectron spectroscopy (XPS), temperature-programmed reduction of H_2 (H_2-TPR), scanning electron microscope (SEM), N_2 physisorption, and H_2 chemisorption

1.5 Procedure of the research

1.5.1 Conduct literature review.

1.5.2 Experimental set up (chemicals and apparatus).

1.5.3 Preparation of Co/γ-Al_2O_3 and the addition of promoters with Co/γ-Al_2O_3 catalysts by solid-state reaction with gibbsite and calcined at 650 °C.

1.5.4 Test the all catalysts in CO_2 hydrogenation reaction.

1.5.5 Characterizations of the all catalysts by using XRD, XPS, H_2-TPR, N_2physisorption, and H_2 chemisorption.

1.5.6 Discussion and conclusion.

1.5.7 Write thesis for publication.

CHAPTER II

THEORY AND LITERATURE REVIEWS

2.1 Carbon dioxide hydrogenation reaction

Currently, the exhaust gas, carbon dioxide (CO_2), is increased due to enhancement the efficiency of industry and spending human life. The drastic increase in CO_2 concentration is the main cause of the increase in earth temperature, sea-levels rising and other natural catastrophes. Hence, the scientists developed efficient CO_2 capture and utilization systems to curb CO_2 emissions. Indeed, the hydrogenation of CO_2 not only reduces the increasing CO_2 of buildup but also produces fuels and chemicals as shown in Figure 2.1. The products of CO_2 hydrogenation such as methanol, dimethyl ether (DME), and hydrocarbons, are excellent fuels in internal combustion engines, and also are easy for storage and transportation. Furthermore, methanol and formic acid are raw materials and intermediates for many chemical industries.

$$
\begin{aligned}
CO_2 + H_2 &\longrightarrow CH_4 \\
&\longrightarrow Hydrocarbons \\
&\longrightarrow CO \\
&\longrightarrow Higher\ alcohols \\
&\longrightarrow CH_3OH \\
&\longrightarrow CH_3OCH_3 \\
&\longrightarrow HCOOH \\
&\xrightarrow{R_2NH} HCONH_2
\end{aligned}
$$

Figure 2.1 Product from CO_2 hydrogenation [15]

$$CO_2 \xrightarrow{H_2} CO \xrightarrow{H_2} Straight\ chain\ hydrocarbon$$

$$\xrightarrow[hydrogen\ transfer]{cracking} Small\ olefin \xrightarrow[hydrogen\ transfer,\ isomerization]{transmutation,\ oligomerization} C_2 - C_{10}\ olefin$$

$$\xrightarrow[hydrogen\ transfer]{cyclization} A_6 - A_{10}\ aromatic$$

Figure 2.2 The overall reaction scheme in CO_2 hydrogenation [16].

In the past decades, several researches have studied the CO_2 hydrogenation. The hydrogenation of CO_2 on metal catalysts occurred through mechanism in which CO_2 was firstly converted to CO by the reverse water gas shift (RWGS) reaction, and then CO was hydrogenated to hydrocarbons. Thus, the chain mechanism of hydrocarbon synthesis from CO_2 was similar to the Fischer-Tropsch synthesis (FTS) reaction. The CO_2 hydrogenation to hydrocarbons proceeded through formation of CO as intermediate. The overall reaction scheme in hydrogenation of CO_2 can be shown in Figure 2.2.

$$CO_2 + 4H_2 \rightarrow CH_4 + H_2O \ ;\ \Delta H_{298K} = -252.9\ kJ/mole \qquad 2.1$$

The CO_2 hydrogenation reaction is interesting as a production of synthetic natural gas (SNG) which is modified from the FT synthesis, where CO_2 is used instead of CO. The formation of methane (CH_4) from CO_2 hydrogenation reaction, as illustrated in equation 2.1, requires a ratio of H_2/CO_2 equal to 4:1. This reaction is exothermic reaction and spontaneous at room temperature ΔH_{298K} = -252.9 kJ/mole, ΔG_{298K} = -130.8 kJ/mole. The Gibbs free energy increases rapidly with temperature and becomes positive when the temperature over 500 °C. By this condition, it would have led to the reverse reaction of CO_2 hydrogenation, which is a reforming of

methane. However, an 8-electron process is required to reduce the fully oxidized carbon to methane and there are significant kinetic limitations which require a catalyst to achieve acceptable rates and selectivities [15,17].

$$CO_2 + H_2 \rightarrow CO + H_2O; \Delta H_{573K} = 38 \text{ kJ/mole} \quad 2.2$$

$$CO + 3H_2 \rightarrow CH_4 + H_2O; \Delta H_{573K} = -166 \text{ kJ/mole} \quad 2.3$$

Many researchers believed [15,17,18] that carbon monoxide is a critical intermediate in CO_2 hydrogenation. The following reactions has summarized the overall reduction process into two steps ,the initial reduction of CO_2 to CO via the reverse-water gas shift (RWGS) reaction followed by the conversion of CO to methane via an FT reaction, which can be shown in equation 2.2 and 2.3, respectively.

Yaling Zhao et al. [19] reported a kinetics model of the CO_2 hydrogenation over iron-nickel catalysts. There are five elementary reactions of light alkenes synthesis from CO_2 hydrogenation consist of reactant adsorption, chain initiation, chain growth, chain termination and the product desorption, alkenes re-adsorption and secondary reaction

I. Reactant of adsorption occurred on the catalyst surface are:

$$CO_2 + (s_1) \longleftrightarrow CO_2(s_1) \quad 2.4$$

$$CO_2(s_1) + (s_1) \longleftrightarrow CO(s_1) + O(s_1) \quad 2.5$$

$$H_2 + (s_1) \longleftrightarrow 2H(s_1) \quad 2.6$$

Here, (s_1) shows the vacant activity sites of catalyst

II. Chain initiation

$$CO(s_1) + H_2 \longleftrightarrow H_2CO(s_1) \quad 2.7$$

$$H_2CO(s_1) \quad + \quad H_2 \quad \longleftrightarrow \quad CH_2(s_1) \quad + \quad H_2O \qquad 2.8$$

III. Chain growth with metal-alkyl bond insertion :

$$CH_2(S_1) \quad + \quad C_nH_{2n+1}(s_1) \quad \longleftrightarrow \quad C_{n+1}H_{2n+3}(s_1) + (s_1) \qquad 2.9$$

or with metal-alkylidene bond

$$CH_2(S_1) \quad + \quad C_nH_{2n}(s_1) \quad \longleftrightarrow \quad C_{n+1}H_{2n+2}(s_1) \quad + \quad (s_1) \qquad 2.10$$

IV. There are many of routes for chain termination :

The formation of alkene products occurred after $C_nH_{2n+1}(s_1)$.

$$C_nH_{2n+1}(s_1) \quad \longleftrightarrow \quad C_nH_{2n} \quad + \quad H(s_1) \qquad 2.11$$

or the formation of the alkane products :

$$C_nH_{2n+1}(s_1) \quad + \quad H_2 \quad \longleftrightarrow \quad C_nH_{2n+2} \quad + \quad H(s_1) \qquad 2.12$$

$$C_nH_{2n+1}(s_1) \quad + \quad H(s_1) \quad \longleftrightarrow \quad C_nH_{2n+2} \quad + \quad 2(s_1) \qquad 2.13$$

V. Last step, alkenes re-adsorption and secondary reaction play an important role in the product distribution of CO_2 hydrogenation

$$C_nH_{2n}(s_1) \quad \longleftrightarrow \quad C_nH_{2n} \quad + \quad (s_1) \qquad 2.14$$

In the past, scientists have continuously studied a catalytic system upon VIIIB metals (e.g., Co, Fe, Ni, Ru and Rh) supported on various oxides for the CO_2 hydrogenation. Moreover, they also focused on the optimization and improvement of catalysts for specific applications such as active component, support, and promoter which these have important effects on the catalyst performance and structure.

2.1.1 Active element for CO_2 hydrogenation

Metal oxide supported catalysts have been studied in many researches for investigating the CO and CO_2 hydrogenation reaction which determine a variety of

products. Hydrogenation of CO_2 to methane has been investigated using alternative suitable catalysts as group VIIIB metals (e.g. Co, Ni, Ru, Rh, Pt, and Fe). Noble metals such as Rh, Ru, Pt, and Ir encourage CO_2 hydrogenation performance due to high stability, high reactivity, and high selectivity of CH_4 and less sensitive to coke deposition. Nevertheless, noble metals are expensive and not match available. In this case, an addition of dopants and supports is a good alternative to avoid the high cost of using these precious metals. Likewise, transition metals such as Fe, Co, and Ni are also one of alternatives for CO_2 hydrogenation because these metals are not only cheaper but also good reactivity.

Hitoshi Kusama *et al*. [20] applied Rh/SiO_2 catalysts with Rh loading ranging from 1.0 to 10.0 wt.% prepared by impregnation method. The effect of metal loading on the reactivity on the CO_2 hydrogenation was studied. The results found that the low loaded Rh catalyst (1 wt.% Rh/SiO_2) gave the CO as a main product, while CH_4 was dominantly produced on the higher loaded Rh (10 wt.% Rh/SiO_2). The result of H_2 chemisorption and FT-IR conducted showed that the concentration of Rh particles on SiO_2 surface had a significant influence on the reactivity for CO_2 hydrogenation.

Improved catalyst by synthesis of titania-nanotubes (Tnt) of modifying Kasuga's process and later being uniformly immobilized Pt nanoparticles on the Tnt with photochemical deposition (PCD) method has been studied by Kuo-Pin Yu *et al*. [21]. The result found that the surface area of Tnt was 191 m^2/g and slightly decreased the deposition of Pt (187 m^2/g) which uniformly dispersed of Pt nanoparticles (about 1–3 nm) on Tnt as demonstrated by TPR and XPS. The CO_2-TPD results indicated that improved catalyst with Tnt enhanced CO_2 adsorption better

than TiO_2. Moreover, the residual sodium in the Tnt might also be responsible for the CO_2 adsorption. The *in situ* FT-IR indicated that the Pt/Tnt was a highly active catalyst for the CO_2 hydrogenation into methane production at low temperature.

Mechanical combination of Rh/-Al_2O_3 and Ni/AC catalysts, which prepared separately, was recently reviewed by Colas Swalus *et al*. [22]. The 1 wt.% Rh/-Al_2O_3 catalyst was prepared by incipient wetness impregnation and the 1%Ni/AC catalyst was prepared by aqueous hydrazine reduction. Then, both catalysts were mixed by mechanical mixing. The cooperated between both catalysts in CO_2 methanation which the 1 wt.% Rh/-Al_2O_3 was efficient in CO_2 adsorption. On the other hand, the 1 wt.% Ni/AC catalyst was able to absorb a high quantity of hydrogen. The resulted show that CH_4 formation from mixture Rh/-Al_2O_3 and Ni/AC, which contained no chemical contamination or formation of new structures, is higher when compared with the pure catalysts.

2.1.2 Promoter effects

The addition of the promoters is the simplest method that increases the rate per site per second. A small amount of promoters is added to catalyze materials to improve their activity, selectivity and/or stability [9]. It is generally accepted that promoter may influence these useful effects in several manners. These promoters are divided into two types: (i) noble metal (Pt, Ru, Rh, Pd) and (ii) non-noble metal (Mn, Fe, Ce, Cu, Mo, Mg, B, K). However, promoters only show beneficial in a limited concentration range as an addition of excessive amount of promoter could lead to a complete decoration of the active surface on the catalysts, and a decrease of the catalyst activity. Therefore, the level of promoters, which were added to modify a catalyst, could be either as a promoter or a poison.

Earlier, Nickel was used as catalyst for CO_2 hydrogenation but it was found that the major problem of Ni-based catalyst is deactivation at low temperature owing to the interaction of metal particles with CO and formation of mobile nickel subcarbonyls [23]. Consequently, improved Ni-based catalysts performance has been studied by Anmin Zhao *et al*. [4]. They studied the effect of the Mn additive on Ni/Al_2O_3catalysts prepared by co-impregnation to specifically improve its catalytic activity and stability. Ni/Al_2O_3 catalyst, with Ni loading of 24 wt%, were modified by different amounts of Mn ranging (1-3 wt%). Addition of Mn to Ni/Al_2O_3 catalysts increased surface area but slightly decrease NiO crystallite size causing higher activity and stability. CO_2 conversion and CH_4 formation rate were changed depending on operation temperature, pressure, weight hourly space velocity (GHSV). The condition test was accomplished at 280–450 $^{\circ}$C, 30000–45000 $mL \cdot g^{-1} \cdot h^{-1}$and around 2.0 MPa.

Taraknath Das *et al*. [6] studied that individual metal loadings and the method of depositing the individual metals over alumina supported. Comparison of 15% Co/Al_2O_3 with 15%Fe/Al_2O_3 resulted that cobalt supported catalyst had higher catalytic activity than iron supported catalyst. Besides, substitution of Co with Fe, with the same total metal loading of 15%, had found that the alumina supported Co catalysts was promoted by Fe and an appropriate amount of Co and Fe was required for the highest CO_2 conversion and CH_4 yield. The order of depositing Co and Fe on the alumina support was also important due to effect of the crystallite size of the Co–Fe alloy on the alumina support.

Robert W. Dorner *et al*. [24] studied the improved catalyst by the addition of ceria on $Fe/Mn–Al_2O_3$ catalyst. The result indicated that the addition of Ce (at low Ce levels) to a $Fe/Mn–Al_2O_3$ catalyst leads to a small improvement in CO_2 conversion

and product selectivity. The large addition of Ce that ceria forms on top of the iron particles, leading to blocking chain-growth active sites on the iron.

Sudhanshu Sharma *et al*. [25] reported an investigation of CO_2 methanation by catalysts consisting of CeO_2 doped with Ni, Co, Pd, or Ru. The best catalysts were $Ce_{0.95}Ru_{0.05}O_2$ and $Ce_{0.96}Ru_{0.04}O_2$ as the highest activity and selectivity of CH_4 at 450 °C. There is no CO formed up to this temperature. Ce doped with Ni or Co catalysts generated either the CO_2 methanation or the reverse water–gas shift reaction (RWGS). While Pd-doped Ce produced only CO production as generated only RWGS reaction.

Previously, metal oxide such as Ni, Co, Mn, Fe, Ce were used as catalysts for the CO_2 hydrogenation but they had lost of catalytic ability after a few hours. Thereby, noble metals were incorporated to solve this problem. Wei Chu et al. *et al*. [26] studied about calcination temperature and Pt promoted Co/γ-Al_2O_3 catalysts for Fischer-Trosch synthesis (FTS). The result revealed that calcination at temperature ranging 473–773 K and promotion of small amounts of Pt had no significant influence on the size of Co_3O_4 crystallites in γ-Al_2O_3supported cobalt. Nonetheless, promotion with 0.1 wt% of Pt, which significantly enhanced cobalt reduction, led to an increase in the FTS rate and a decrease in C_{5+} hydrocarbon selectivity.

Jung-Nam Park *et al*. [17] prepared intermixed Pd and Mg sites catalysts using reverse microemulsions for CO_2 methanation. The Pd-Mg/SiO_2 catalyst showed higher selectivity for CH_4 (95%) and greater CO_2 (59%) and H_2 conversion compared to several other catalyst preparations. When replacing the Mg with Fe or Ni, it had given the high activity; however, the Fe-containing catalyst had little CH_4 selectivity.

2.1.3 Supported effects

The supports may influence with the important both catalytic activity and selectivity for the reaction. In addition, they also control the particle morphology. The supports such as SiO_2, TiO_2, ZrO_2, MgO, or Al_2O_3 are used material supports which encourage fine dispersion crystallites of metal, since these oxides have suitable properties such as high surface area, numerous acidic/basic sites, and interaction between support and metal [27].

Kowalczyk *et al*. [28] studied the effect of the type of support (Al_2O_3, $MgAl_2O_4$, MgO, and Carbon) and metal loading in on the catalytic performance of Ru nanoparticles for carbon monoxide and carbon dioxide methanation at very low CO_x/H_2 ratio. The results demonstrated that the properties of ruthenium surfaces showed by TOFs proved to be dependent on the kind of support material and metal dispersion. The following order of TOFs was obtained: Ru/Al_2O_3 > $Ru/MgAl_2O_4$ > Ru/MgO > Ru/C, for CO and CO_2 hydrogenation which are based on dispersion of metal. When compare Ni-based system with ruthenium surfaces at steady state conditions of temperature (220 °C) and gas composition (4000 ppm of CO_x), reaction rates for a highly loaded Ru/Al_2O_3 sample are about 8 times for CO hydrogenation and about 10 times for CO_2 hydrogenation.

Guilin Zhou *et al*. [29] exhibited to develop new mesoporous catalysts for CO_2 catalytic hydrogenation toward methane production. The properties of Co/KIT-6 and Co/meso-SiO_2 catalysts were investigated by XRD, TEM, and BET and indicated that these catalysts have mesoporous structures with well-dispersed Co species. The Co/KIT-6 catalyst has a higher CO_2 catalytic hydrogenation activity than the Co/meso-SiO_2 catalyst. Additionally, the Co/KIT-6 catalyst was more stable than the Co/meso-

SiO_2 catalyst at high reaction temperatures which the CH_4 selectivity could be retained at 100% until 280 °C and slightly decreased when the reaction temperature was higher than 280 °C.

2.2 Alumina (Al_2O_3)

Alumina is solid oxide of aluminum and has chemical formula as Al_2O_3. Several phase transitions have been specified including the eta (η), theta (θ), kappa (κ), chi (χ), delta (δ), and gamma (γ) alumina. Transition aluminas are widely used as catalysts, catalyst supports, and membranes due to their high surface area, mesoporosity, and surface acidity [30]. The nature of product occurred depending on parameters such as heating rate and calcination temperature.

Gibbsite, which showed properties in Table 2.1, is one of the three component aluminum minerals and has chemical formula $Al(OH)_3$. The phase transformation has been studied to role in calcination gibbsite $\longrightarrow$ boehmite (γ-AlOOH) $\longrightarrow$ γ-alumina (γ-Al_2O_3) $\longrightarrow$ δ-alumina (δ-Al_2O_3) $\longrightarrow$ θ-alumina (θ-Al_2O_3) $\longrightarrow$ α-alumina (α-Al_2O_3) as shown in Figure 2.3. Each transition phase can be clearly distributed by powder X-ray diffraction pattern [31].

The γ-alumina is significant a material for industrial. It is used as a catalyst support for automotive and industrial catalyst such as fine chemical, catalyst for petroleum refining, and the most important ceramic oxides. In the last decades, there are several researches about preparation of γ-alumina that indicates the reaction sequence depending on many factors such as the physicochemical properties of the initial raw (untreated) material [33,34,35] (particle size, shape,

substituting elements etc.), the circumstances of the heat treatment (temperature, heating rate, composition of the atmosphere, pressure etc.) [34].

From Figure 2.3 that summarizes the pathways of gibbsite thermal decomposition. Gibbsite decomposes to oxide above the temperature of 300 °C, heating up gibbsite results to transformation to boehmite and χ-alumina simultaneously. Over 200 °C gibbsite loses two moles water and transformed into oxihydroxide boehmite. Boehmite decomposes into transitional alumina at 500 °C. The last step of the pathway is the formation of corundum at 1050–1100 °C. All of decomposition role end by the formation of co-rumdum (α-alumina).

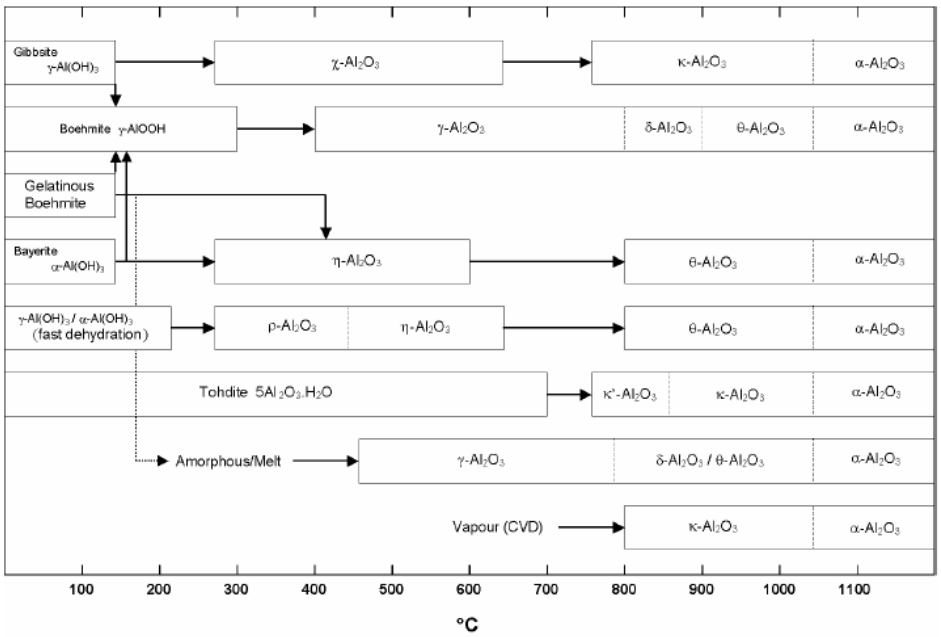

Figure 2.3 Transition sequences of the alumina from hydroxide [31]

Table 2.1 Properties of gibbsite [32]

General Information	
Chemical Formula:	$Al(OH)_3$
Composition:	Molecular Weight = 78.00 g/mol
	Aluminum 34.59 % Al 65.36 % Al_2O_3
	Hydrogen 3.88 % H 34.64 % H_2O
	Oxygen 61.53 % O
	100.00 % 100.00 % = TOTAL OXIDE
Association:	Diaspore, Bohmite, Corundum, Kaolinite, Goethite
Environment:	Lateritic soils developed on aluminous rocks in areas of high rainfall.
Gibbsite Crystallography	
Axial Ratios:	a:b:c =1.7043:1:1.9169
Cell Dimensions:	a = 8.641, b = 5.07, c = 9.719, Z = 8; beta = 94.566° V = 424.44 Den(Calc.)= 2.44
Crystal System:	Monoclinic – Prismatic H-M Symbol (2/m) Space Group: P 21/n
X Ray Diffraction:	By Intensity (I/Io): 4.82(1), 4.34(0.4), 4.3(0.2)
Physical Properties	
Cleavage:	{001} Perfect
Color:	Bluish, Green, Green white, Gray, Gray white.
Density:	2.3 - 2.4, Average = 2.34
Diaphaneity:	Translucent to transparent

Physical Properties	
Hardness:	2.5-3 - Finger Nail-Calcite
Luster:	Vitreous – Pearly
Streak:	White

The properties of alumina (Al_2O_3), which displayed in Table 2.2 make it a very attractive material because of great hardness, high thermal resistance, high chemical stability, high melting temperature, high degree of refractoriness, and high dielectric strength. Because there are many advantages of alumina; for example, it retains greater strength which can be made into beneficial products, such as the refractory material in furnace, crucible for the jewelry industry, spark plug for automotive industry, and part of the replacement organs.

Table 2.2 Properties of Al_2O_3 are summarized [36].

mechanical	Unit of measure	94%Al_2O_3	96%Al_2O_3	99.5%Al_2O_3
Density	g/cc	3.96	3.72	3.89
Porosity	%	0	0	0
Color	-	white	white	ivory
Flexural strength	Mpa	330	345	379
Elastic modulus	Gpa	300	300	375
Shear modulus	GPa	124	124	152
Bulk modulus	Gpa	165	172	228
Poisson's ration	-	0.21	0.21	0.22
Compressive strength	MPa	2100	2100	2600

mechanical	Unit of measure	94%Al_2O_3	96%Al_2O_3	99.5%Al_2O_3
Hardness	kg/mm^2	1175	1100	1440
Fracture toughness K_{IC}	$MPa.m^{1/2}$	3.5	3.5	4
Maximum use temp.	°C	1700	1700	1750
Thermal				
Thermal conductivity	W/m.K	18	25	35
Coefficient of thermal expansion	10^{-6}/°C	8.1	8.2	8.4
Specific heat	J/kg.K	880	880	880
Electical				
Dielectric strength	ac-kV/mm	16.7	14.6	16.9
Dielectric constant	at 25 °C, 1MHz	9.1	9	9.8
Dissipation factor	at 25 °C, 1MHz	0.0007	0.0011	0.0002
Volume resistivity	Ω.cm	$>10^{14}$	$>10^{14}$	$>10^{14}$

2.3 Cobalt

Cobalt is a naturally occurring element, atomic number 27 and atomic weight 58.93 which is one of the first transition series of Group VIIB of the periodic table. Cobalt is found in the minerals cobaltite, erythrite, and smaltite. It is commonly associated with ores of iron, nickel, silver, lead, and copper. ^{59}Co is the only stable isotope. There are 26 known radioactive isotopes, of which only ^{57}Co and ^{60}Co are commercially important.

Metallic cobalt (Co^0) naturally has two allotropic forms, hexagonal and cubic, which are stable at room temperature. Cobalt is a silvery grey solid at room

temperature. The melting point is 1493 °C (1766 K). The density of cobalt is 8.9 g/cm^3 at room temperature (20 °C). Cobalt can be dissolved in dilute acids and ultrafine metal cobalt powder can be dissolved in water at 1.1 mg/l [36].

There are three valance states of cobalt (0, +2, +3). Co^{+2} is more stable than Co^{+3} which oxidizes water and liberates oxygen [19]. There are two stable bulk of cobalt oxide such as fcc-type rocksalt structure of CoO (Co^{+2}) and cubic spinel structure of Co_3O_4 (Co^{+3}) at room temperature. The thermodynamically stable form of cobalt oxide at room temperature is the Co_3O_4 spinel structure, which is specially more interested than the other oxide forms due to its various application such as sensor, heterogeneous catalyst, lithium ion batteries, and magnetic materials in energy storages [19].

From other researches, researchers had studied all the group VIII elements that display considerable activity for CO_2 hydrogenation. Among all the catalysts, Co, Fe and Ru present the highest activity [3,5,6,8,12]. Besides, cobalt has several benefits compared to Ru such as high activity for CO_2 hydrogenation, high selectivity to linear products, more stability towards deactivation, low activity towards water-gas shift (WGS) reaction and low cost [37,38].

Table 2.3 Properties of Cobalt

General Information	
Atomic Number	27
Symbol	Co
Atomic Weight	58.9332
Electron Configuration	[Ar] $4s^2 3d^7$
Element Classification	Transition Metal
Oxidation States	0, +3, +2
Physical Properties	
Density	8.9 g/cm^3
Molar volume	6.67 cm^3
Young's modulus	209 GPa
Bulk modulus	180 GPa
Poisson's ratio	0.31
Hardness	
- Mineral	5.0 (no units)
- Brinell	700 MN m^{-2}
- Vickers	1043 MN m^{-2}
Melting Point	1768 [or 1495 °C (2723 °F)] K
Boiling Point	3200 [or 2927 °C (5301 °F)] K
Electrical resistivity:	6 $x10^{-8}$ Ω.m
Thermal conductivity	100 W/m.K

Crystal structure	
Space group	P63/mmc (Space group number: 194)
Structure	hcp (hexagonal close-packed)
Cell parameters	*a*: 250.71 pm, b: 250.71 pm, c: 406.95 pm α: 90.000°, β: 90.000°, γ: 120.000°
Thermal Properties	
Enthalpy of fusion:	16.2 kJ/mol
Enthalpy of vaporisation:	375 kJ/mol
Enthalpy of atomisation	425 kJ/mol
Specific Heat @20°C	0.456 J/g mol
Heat of fusion (ΔH_{fus})	15.48 kJ/mol
Evaporation Heat	389.1 kJ/mol
Latent heat of vaporization	6276 kJ/g
Debye Temperature	385.0 K
First Ionizing Energy	758.1 kJ/mol

Though the cobalt (III) oxide catalyst is used for the hydrogenation of CO_2; however, the active site for this reaction must be especially cobalt metal. Thus, the reduction process is required. The reduction of Co_3O_4 is a two reaction steps [1]:

First step: $$Co_3O_4 + H_2 \longrightarrow 3CoO + H_2O \qquad 2.15$$

Second step: $$CoO + H_2 \longrightarrow Co \quad H_2O \qquad 2.16$$

The interaction between the metal and the support considerably affects the properties of the catalyst, leading to enhancement of reducibility. Previous researches, found that the position of reduction peaks depended on the kind of supports [4], promoters [6,8,26], and calcination temperature [26]. Gary Jacobs *et al*. [22] investigated a two-step reduction process involving Co_3O_4 to CoO and CoO to Co^0 transformations over standard calcined catalysts was observed and quantified over all catalysts exhibiting both weak interactions (Co/SiO_2) and strong interactions (Co/Al_2O_3) with the support. Improvement of catalyst activity can be achieved by addition of a second metal as promoter that is stable under reaction conditions. Temperature reduction of various supported cobalt catalysts was demonstrated in Table 2.4.

However, the scientists studied the addition of promoters which can also enhance reducibility of cobalt (III) oxide. From the previous reports, promotion with platinum resulted in a lower temperature shift of the peaks of reduction of CoO to metallic cobalt thus, added Pt can enhance cobalt reduction for both Co_3O_4 to CoO and CoO to Co^0 [26]. Sardar Ali *et al*. [38] reported an improve alumina supported cobalt with incorporating difference amount of iron. The results found that the addition of iron up to 30% into cobalt catalysts increased the reduction while, the iron-riched bimetallic catalysts showed an opposite trend catalysts.

Table 2.4 shows temperature-program-reduction (TPR) of each research.

Catalysts	Temperature Reduction (K)		Ref.
	First step	Second step	
Co/Al_2O_3	780	923	[39]
Co/SiO_2	780	723	[39]
Co/TiO_2	573	773	[40]
Co/CNT[a]	603	701	[41]

a: carbon nano tube

2.4 Solid state reaction

The solid-state reaction is the most extensively used method for the preparation of polycrystalline solids, which are a mixture of solid starting materials. However, the solids do not react with another at room temperature and it is important to heat them up to the higher temperatures (1000 to 1500 °C) in order to initiate the reaction at an appreciable rate. The factors which affect to rate of a solid state reaction include, surface area, structure properties, and condition reaction of the solids.

A solid state reaction, called a solvent-free reaction, is chemical reaction without solvents. Normally, the reactants are mixed in solvent before the reaction can occur. After the reaction is completed, the products are removed from solvent. Advantages and disadvantages of solid-state reaction were shown in Table 2.1

Recently, the formation of kinetic equation had been studied by the processes control the rates of solid-state reactions dependent on nucleation, interface advance (growth), and diffusion.

Table 2.5 Advantage and disadvantage of solid state reaction

Advantage	Disadvantage
1. The simplest	1. irregularly disperse metallic over support
2. Cheaper and convenient	2. decompose of material
3. use less solvent and contamination	
4. give high yield of product	

2.4.1 Nucleation [42]

Nucleation is the initial creation of a new and separable product from the solid reactant. It began at only a relatively small number of nucleation sites about the scale of 10-1000 atoms. Conclusively, these possess essentially improved local reactivity. Although this step is crucial for several geochemical and mineralogical processes, the development of nucleation is quiet at its beginning. The result of nucleation process, maybe requiring many steps, is the formation of the active reactant-product interface at which reaction happens during its subsequent advance into unchanged reactant since the nucleus grows.

2.4.2 Interface advance (growth) [42]

Surface processes and transport processes are two of the main processes of atomic processes that occur during crystal growth. In details, surface processes composed of attachment, detachment, and movement of atom while transport and diffusion of atom away from surfaces are compositions of transport processes. Since the transport mechanism could guarantee homogeneity by acting fast and with the

rate of growth were surface controlled, the concentration gradient of reactant in the medium around the growing phase would be very diminutive.

2.4.3 Diffusion [42]

Diffusion is mass transport process that is a important mechanism in solid state reactions. Besides, it is a main control in a structure that is not reorganized by the chemical change. Fick's law controls the reaction rates. J_A is the proportional to the concentration gradient of A which can be shown as :

$$J_A = -D_A \frac{\partial[A]}{\partial x} \qquad 2.17$$

Where J_A is the flux of component A

x is the distance measured normal to the surface that flux passes through

D_A is diffusion coefficient

$[A]$ is concentration of component A

The driving force for the flux showed in equation 2.17. Nevertheless, the chemical potential gradient is preferable for the exhibition of diffusion flux. For the situation when a flux diffuses across two different phase, there will be a discontinuity in concentration across the phase boundary (e.g. a discontinuity in $\partial[A]/\partial x$).

There are three kinds of diffusion that occur in solid state reaction as surface diffusion, grain boundary diffusion, and bulk diffusion as illustrated in Figure 2.4. Surface diffusion occurs in a two-dimensional interface between the crystal grain and nonsolid media. Grain boundary diffusion occurs along the boundaries between solid phases. Bulk diffusion occurs within the lattice sites of the solids.

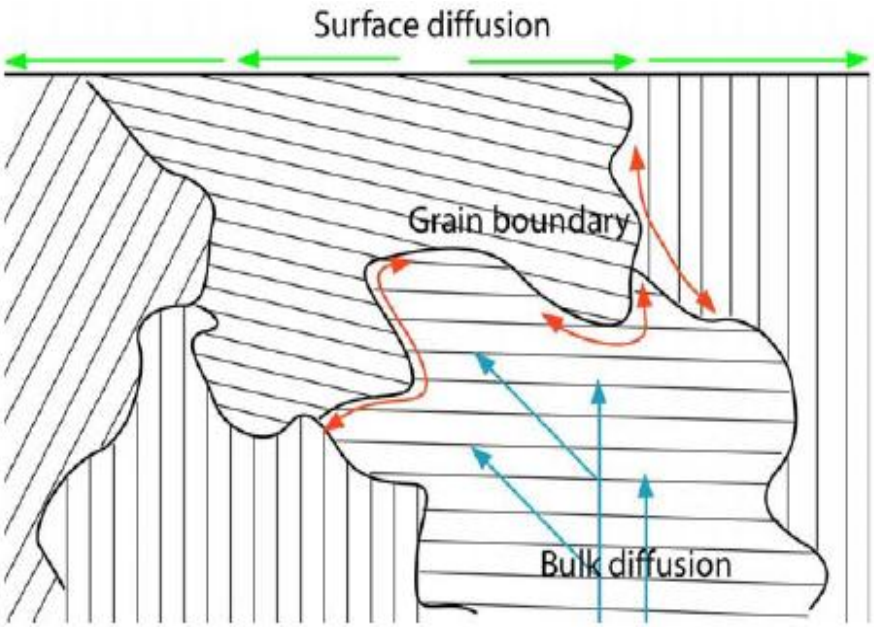

Figure 2.4 Three kinds of diffusion in solid state as surface diffusion, grain boundary diffusion, and bulk diffusion [42].

Normally, surface diffusion is the fastest followed by grain boundary diffusion, while bulk diffusion is the slowest. For solid-state reaction, the main factor manipulation the values of diffusion coefficient is the structure of material. The diffusion in solid is dependent on temperature that illustrated by Arrhenius law.

$$D_A = D_0 \exp\left(-\frac{E_a}{RT}\right) \qquad 2.18$$

Thereby, $\ln(D_A)$ is a linear function of $1/T$ if the reaction mechanism remains constant?

CHAPTER III

EXPERIMENTAL

This chapter composed of three parts: (i) the catalyst preparation, (ii) catalyst characterization and (iii) catalyst test in CO_2 hydrogenation. The first section describes preparation of catalysts promoted and non-promoted cobalt catalyst. The second section ,the catalysts were characterized by X-ray diffractrometer (XRD), H_2 chemisorption, X-ray photoelectron Spectroscopy (XPS), N_2 physisorption, temperature programmed reduction (TPR), and scanning electron microscope with energy-dispersive X-Ray analyzing system (SEM-EDX). The last section, their catalytic performances were evaluated in the hydrogenation of CO_2.

3.1 Catalyst preparation

3.1.1 Chemicals

Table 3.1 The chemicals used in this experimental are shown:

Chemicals	Supplier
Alumina(III) hydroxy	Merck KGaA
Cobalt(II) nitrate hexahydrate ≥ 98%	Sigma-Aldrich Co. Lcc.
Cerium (III) acetate 99.9%	Sigma-Aldrich Co. Lcc.
Potassium nitrate	BHD Chemical Ltd.
Manganese (II) acetate ≥ 99%	Sigma-Aldrich Co. Lcc.
Copper (II) nitrate	Sigma-Aldrich Co. Lcc.

3.1.2 Preparation of the addition of second metal in Co/γ-Al_2O_3 catalyst by solid-state reaction.

The Co/Al_2O_3 catalysts were prepared by a solid-state reaction. The catalyst was prepared by a mechanical mixing of a desirable amount of cobalt (II) nitrate hexahydrate as a precursor (15 wt.% loading) and second metal (0.0, 0.5, 1.0, 2.0wt% loading) with gibbsite ($Al(OH)_3$). The mixed materials were dried in an oven at 383 K for overnight. Finally, they were calcined in flowing air at 923 K for 5 h, with a heating ramp of 10 °C•min^{-1}

3.1.3 Preparation of the selected promoter in Co/γ-Al_2O_3 catalyst by incipient wetness impregnation

The Co/Al_2O_3 catalysts were prepared by incipient impregnation to use as a reference. The cobalt catalyst was prepared by impregnation methods using aqueous solution of cobalt (II) nitrate hexahydrate as a precursor (15 wt.% loading). The supports have been incipient impregnate with aqueous solution of cobalt (II) nitrate hexahydrate. Then, dried in an oven at 383 K for 12 h and calcined in air at 923 K for 5 h, with heating rate 10 °C•min^{-1}

3.2 Characterization of catalysts

3.2.1 X-Ray Diffraction (XRD)

Powder X-ray diffraction (XRD) was performed to determine the bulk phase of catalysts by SIEMENS D 500 X-ray diffractometer connected with a computer with Diffract ZT using Cu Kα radiation. XRD patterns were recorded over a 2θ range of 10°–80° and a step size of 0.02. The crystallite size was evaluated from Scherrer's equation and corumdum (α-alumina) was used as a standard.

3.2.2 X-ray Photoelectron Spectroscopy (XPS)

X-ray Photoelectron Spectroscopy (XPS) was measured by AMICUS spectrometer equipped using a Mg K-α X-ray radiation at 15 kV and current of 12 mA. The pressure analysis chamber was less than 10^{-5} Pa. The AMICUS system is controlled using the AMICUS "VISION 2" software.

3.2.3 H_2 temperature-programmed reduction (H_2-TPR)

H_2 temperature-programmed reduction (H_2-TPR) was carried out to determine the reduction of the catalysts by using a Micrometrics Chemisorb 2750 system.

3.2.3.1 The catalyst sample 0.1 g was used in a quartz U-tube reactor.

3.2.3.2 Prior to the TPR measurements, the catalyst sample was heated up to 723 K in a flowing N_2 at a flow rate of 25 mL•min^{-1}and held at this temperature for 1 h.

3.2.3.3 And then the catalyst sample was cooled down to room temperature in a flowing N_2 at a flow rate of 25 mL•min^{-1}

3.2.3.4 The temperature program reduction was conducted with a gas mixture of 10 vol%H_2 in Ar at a flow rate of 25 mL•min^{-1} and heated from room temperature to 1073 K by a heating rate of 10 °C•min^{-1}.

3.2.3.5 H_2 consumption was controlled by a thermal conductivity detector (TCD).

3.2.4 Scanning Electron Microscope (SEM)

Scanning Electron Microscope (SEM) was performed to study the morphology on the catalyst surface. The SEM of JEOL mode JSM-5410LV was used the secondary electron mode at 15 kV.

3.2.5 Nitrogen physisorption

N_2 physisorption was used to estimate the BET surface area, pore volume and pore size diameter. A Micrometrics ASAP 2020 was used to measure the amount of nitrogen adsorbed for calculated the surface area and pore size distribution according to Brunauer-Emmett-Teller (BET) and Barret-Joyner-Halenda (BJH).

3.2.6 Hydrogen chemisorption

Hydrogen chemisorption was determined by using a Micrometrics Chemisorb 2750 (pulse chemisorption system) and ASAP 2101CV.3.00 software in order to measure the dispersion of metal particles.

3.2.6.1 The catalyst sample was carried out using 0.2 g in glass reactor.

3.2.6.2 Prior to chemisorption, the catalyst sample was reduced in hydrogen at a flow rate of 50 mL•min^{-1} and by heating the catalyst sample to 623 K with a heating ramp of 10 °C•min^{-1} and held at this temperature for 3 h.

3.2.6.3 Then the catalyst sample was cooled down to 373 K and held at this temperature under flowing nitrogen at a flow rate of 30 mL•min^{-1}

3.2.6.4 The catalyst sample was desorbed by using a thermal conductivity detector (TCD).

3.2.7 Inductively coupled plasma (ICP)

Inductively coupled plasma (ICP) was determined the mass concentration of catalysts in solution. The catalysts are at a relatively high concentration and there was not a lot of background mass associated with other elements. Dilutions have to be made more concentrated analysts into the specified range.

3.2 Reaction study of carbon dioxide hydrogenation

3.3.1 Material

Table 3.2 Gas material for test reaction

Chemicals and Reagents	Supplier
High purity grade hydrogen (99.99 vol.%)	Thai Industrial Gases Limited
High purity grade nitrogen (99.99 vol.%)	Thai Industrial Gases Limited
Carbon dioxide in hydrogen (8.80 vol.%)	Thai Industrial Gases Limited

3.3.2 Instrument and Apparatus

Flow diagram of CO_2 hydrogenation catalyst testing is shown in Figure

3.3.2.1 Reactor

The reactor was made from glass (in side diameter 9 mm). The catalyst was replaced within reactor above the quartz wool.

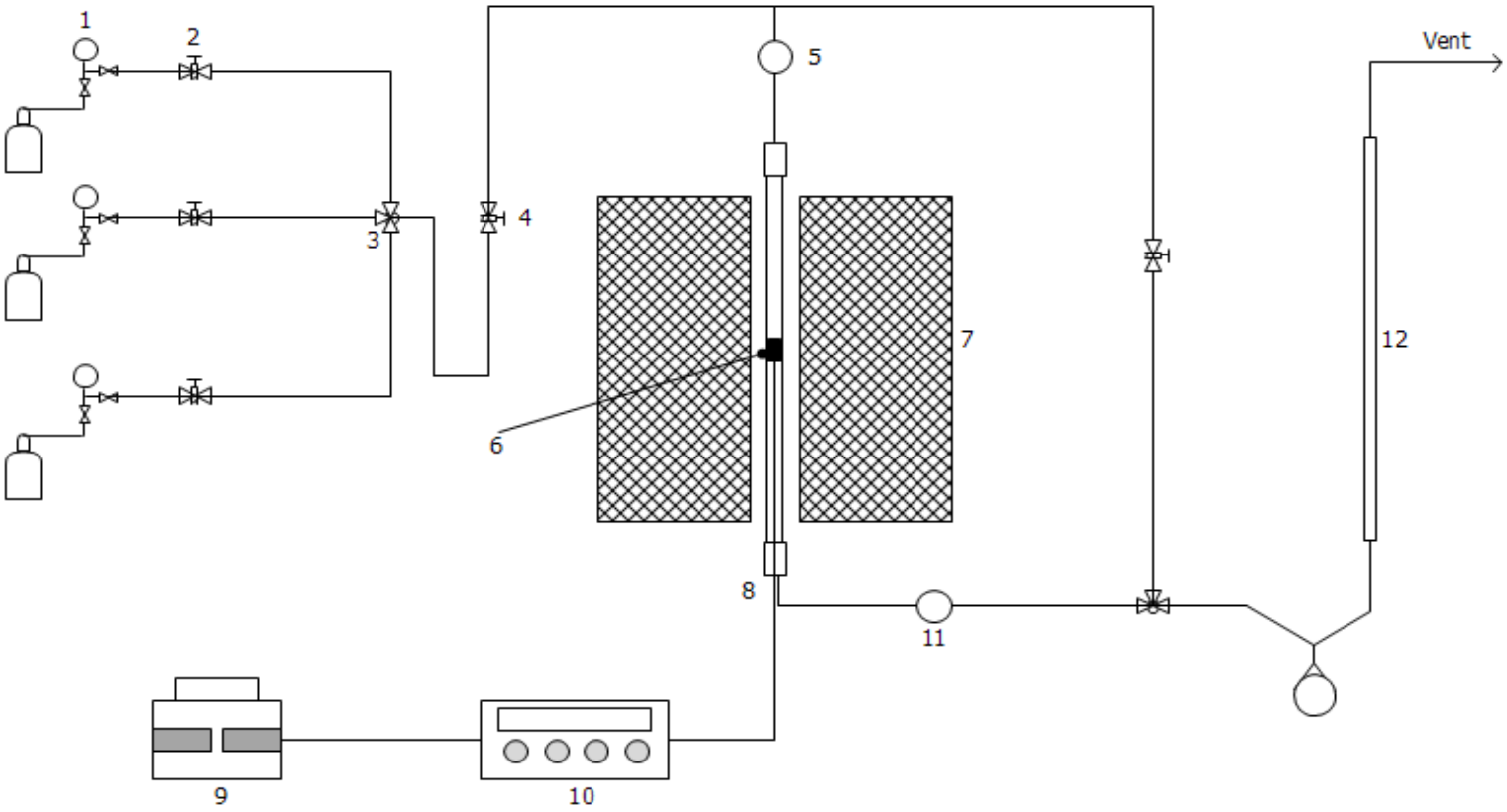

1. Pressure regulator
2. Metering Valve
3. 3-way valve
4. Metering Valve
5. Sampling reactant point
6. Catalyst bed
7. Furnace
8. Thermocouple
9. Variable voltage transformer
10. Temperature controller
11. Sampling product point
12. Bubble flow meter

Figure 3.1 Flow diagram of CO_2 hydrogenation

3.3.2.1 Automatic temperature controller

Automatic temperature controller composed of a magnetic switch which was connected to a variable voltage transformer and a solid-state relay temperature controller which was connected to a thermocouple. Reactor temperature was measured at the bottom of the catalyst bed in the reactor. The temperature control set point is adjustable within the range of 273-1073 K at the maximum voltage 220 volt.

3.3.2.2 Electrical Furnace

The furnace supplied heat to the reactor which could be operated from temperature up to 1073 K at the maximum voltage of 220 volt.

3.3.2.3 Gas controlling system

Reactant for the process was controlled practically using by a pressure regulator, an on-off valve, and the gas flow rates, which were adjusted by using metering valves.

3.3.2.4 Gas Chromatography

The composition of the product and feed which are CO_2, CO, CH_4 and H_2 was analyzed by a Shimadzu GC8A (molecular sieve $5A^0$ and Porapak Q) gas chromatography equipped with a thermal conductivity detector (TCD). The operating conditions for Shimadzu GC8A are shown in the Table 3.3.

Table 3.3 Operating condition of gas chromatograph

Gas chromatograph	SHIMADZU GC-8A
Detector	TCD
Column	Porapak Q, Molecular sieve $5A^0$
-Column material	SUS
-Length	2m
Column	
-Outer diameter	4mm
-Inner diameter	3mm
-Mesh range	60/80
-Maximum temperature	623 K
Carried gas	He (99.999%)
Carried gas flow	40 cc/min
Column gas	He (99.999%)
Column gas flow	40 cc/min
Column temperature	
-initial (°C)	70
-final (°C)	70
Injector temperature (°C)	100
Detector temperature (°C)	100
Current (mA)	80
Analyzed gas	CO, CO_2, H_2, CH_4

3.4 Procedures

Carbon dioxide hydrogenation reaction was evaluated in a glass fixed bed reactor (in side diameter = 9 mm). The thermocouple was put inside the reactor in direct contact with catalysts; therefore, the thermocouple measurement could clearly indicate the temperature of catalyst.

3.3.2 The catalyst was carried out using 0.2 g in glass tube reactor

3.3.3 The catalyst was reduced at 350 °C in flowing H_2 (50 ml/min) for 3 h. And then, the catalysts were cooled to 270 °C in flowing N_2.

3.3.4 After purging with the pre-mixed gas, the reactant gases consisting of H_2/CO_2 molar ratio = 10 (flow rate = 21.3 mL•min−1) were gradually introduced to the reactor.

3.3.5 The gaseous products were analyzed by a gas chromatograph (Shimadzu GC-8A) equipped with a thermal conductivity detector (TCD), a molecular sieve column for H_2, CO, CH_4 and a polapak-Q column for CO_2 separation.

3.5 Research methodology

3.3.6 Part 1: Study of modified Co/Al_2O_3 catalysts by Ce, Mn, K, and Cu by solid-state method

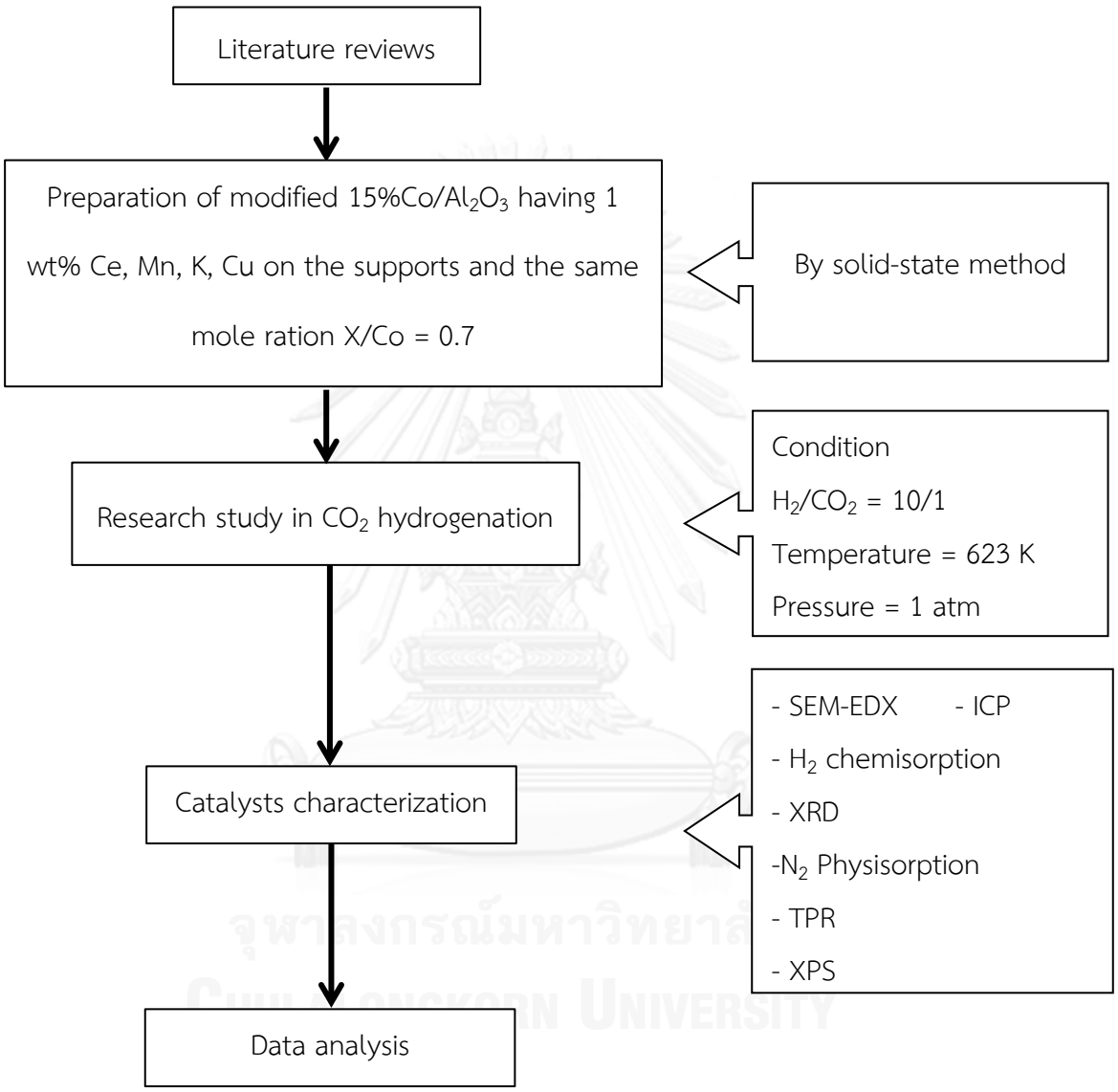

3.3.7 Part 2: Study of the addition difference amount of promoter which give the highest CO_2 conversion Co/Al_2O_3 catalysts by solid-state method

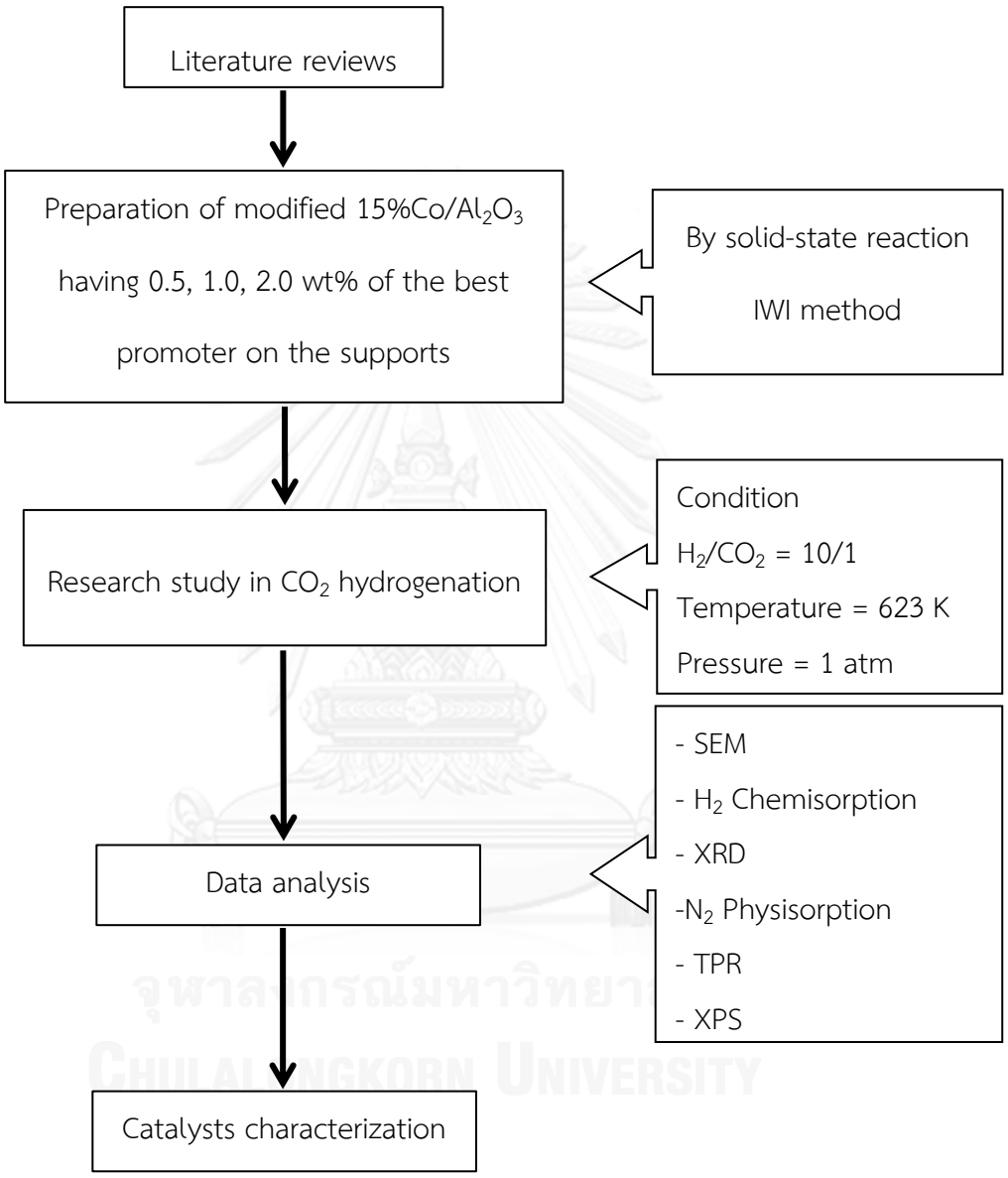

CHAPTER IV

RESULTS AND DISCUSSION

This chapter is divided into two parts: part 4.1 describes the effect of the addition of promoters (K, Mn, Cu, Ce) on the properties of Co/ γ-Al_2O_3 catalysts prepared by solid-state reaction. Part 4.2 describes the effect of different amounts of the selected promoter, which gave the highest CO_2 conversion, on the properties of Co/γ-Al_2O_3 catalysts. The catalytic activity in carbon dioxide hydrogenation reaction and display the catalyst characterization by various techniques such as XRD, XPS, BET, TPR, SEM, and H_2-chemisorption were discussed in this chapter.

4.1 Effect of the addition of promoters on the properties of Co/ γ-Al_2O_3 catalysts.

4.1.1 Characterization of catalysts

4.1.1.1 X-ray diffraction (XRD)

The XRD patterns of the γ-Al_2O_3, the non-promoted Co/γ-Al2O3, and the Co/γ-Al_2O_3 promoted with 1.0 wt.% K, Mn, Cu, and Ce which were prepared by solid-state reaction and incipient wetness impregnation (IWI) method are shown in Figure 4.1. The XRD patterns were recorded over a 2θ range of 10°–80°. The diffraction peaks assigned to the formation of a Co_3O_4 phase were detected at 2θ 18.9°, 31.5°, 37.0°, 44.9°, 55.9, 59.7° and 65.2° [14] in the all catalysts and no characteristic peaks corresponding to other Co species were observed. The peaks at 2θ values of 37°, 43°, 46°, and 67° [4] corresponded to that of γ-Al_2O_3. Additional, peaks corresponding to the second metal added were not observed for all the

promoted catalysts due probably to the very small amount present or they were highly dispersed on the surface of catalysts by generating small particles that were below the detection limit of XRD analysis. However, the Co_3O_4 peaks became broaden after the addition of Mn and Ce. The width of diffraction peak at 2θ at 37° was used to calculate the average size of Co3O4 crystallites by using the Scherer equation and listed in Table 4.1. The average size of Co_3O_4 crystallites in the 1MnCo/γ-Al_2O_3 and 1Ce-Co/γ-Al_2O_3 was estimated to be about 19 and 32 nm, respectively while it was estimated to be about 38 nm in the Co/γ-Al_2O_3. Thus, the addition of small amount of Mn and Ce led to significant changes the dispersion of cobalt over γ-Al_2O_3 support. They were found to be in the order: 1KCo ≈ 1CuCo > Co > 1CeCo > 1Mn-Co.

Figure 4.2 indicates the XRD patterns of the bimetallic with the same mole ratio of X:Co equal to 0.07 (X= Mn, Cu, and Ce) after calcination and preparation by solid-state reaction. The results showed that the diffraction peaks of the second metals were not observed similar to promoted with 1.0 wt.% second metal. Nevertheless, it can be seen that average Co3O4 crystallite size decreased in the following order CuCo (28 nm) > CeCo (26 nm) > MnCo (19 nm). In terms of the effect of preparation method, this results displayed that average Co_3O_4 crystallite size prepared by solid-state reaction were larger than the ones prepared by incipient wetness impregnation method as cobalt loading can enter some pores of γ-Al_2O_3 support after impregnation which was also confirmed by nitrogen physisorption.

Table 4.1 XRD result of the monometallic and bimetallic.

Catalysts	Average Co_3O_4 crystallite size from XRD (nm)
Co/γ-Al_2O_3	38
Co/γ-Al_2O_3-IWI	10
1CeCo/γ-Al_2O_3	32
1CuCo/γ-Al_2O_3	42
1KCo/γ-Al_2O_3	42
1MnCo/γ-Al_2O_3*	19
CeCo/γ-Al_2O_3*	26
CuCo/γ-Al_2O_3*	38

* The same mole ratio of X:Co = 0.07 (X= Mn, Cu, and Ce)

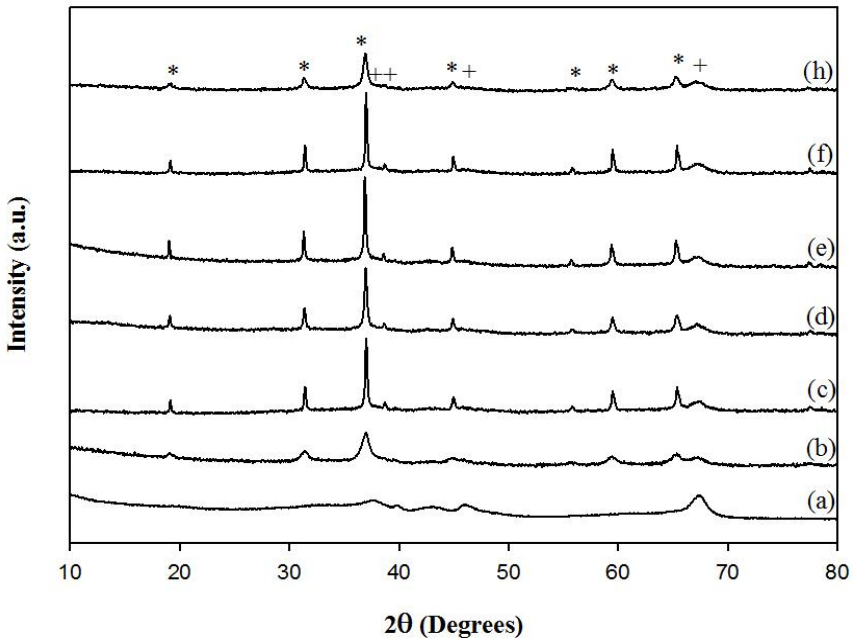

Figure 4.1 XRD patterns for non-promoted, 1wt% promoted catalysts and support after calcination in air at 650 °C for 5 h. (a) /γ-Al_2O_3, (b) Co/γ-Al_2O_3_IWI, (c) Co/γ-Al_2O_3, (d) 1CeCo/γ-Al_2O_3, (e) 1CuCo/γ-Al_2O_3, (f) 1KCo/γ-Al_2O_3, (h) 1MnCo/γ-Al_2O_3, (*) indicates the Co_3O_4 phase and (+) indicates the γ-Al_2O_3 phase from support.

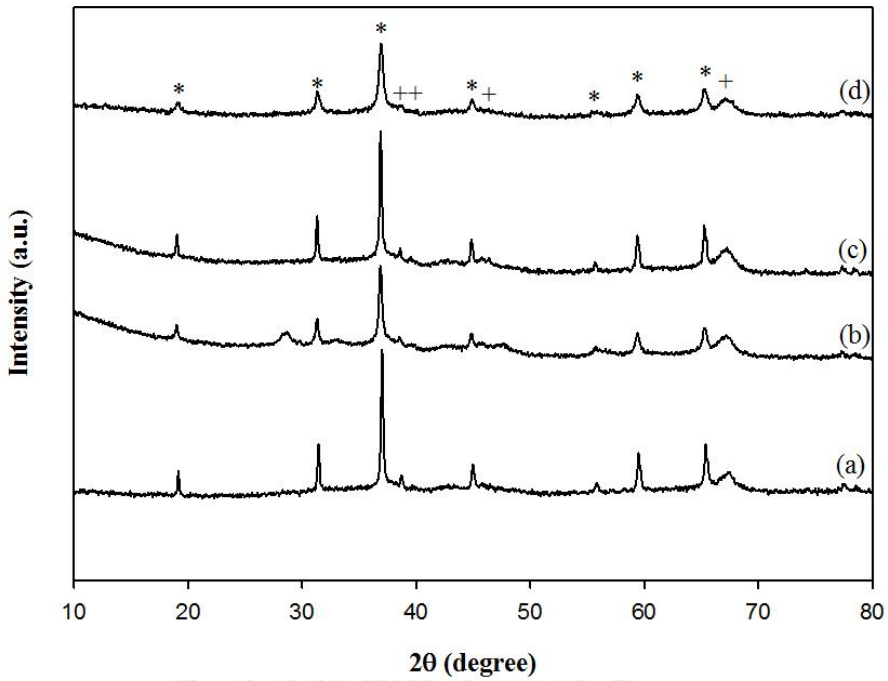

Figure 4.2 XRD patterns for catalysts, which have the same mole ratio of X:Co = 0.07 (X= Mn, Cu, and Ce) after calcination in air at 650 °C for 5 h. (a) Co/γ-Al_2O_3, (b) CeCo/γ-Al_2O_3, (c) CuCo/γ-Al_2O_3, (d) MnCo/γ-Al_2O_3, (*) indicates the Co_3O_4 phase and (+) indicates the γ-Al_2O_3 phase from support.

4.1.1.2 Scanning Electron Microscope (SEM)

The SEM images of the monometallic and bimetallic catalysts on γ-Al_2O_3 support prepared by solid-state reaction and incipient wetness impregnation method are shown in **Figure 4.3**. Form **Figure 4.3**(a) and (b), it is observed that the Co/ γ-Al_2O_3 catalysts prepared by solid-state reaction had smoother surface than another method. Addition of small amount of promoters resulted in litter changes of the morphology of the catalysts. However, some roughness on the surface of the catalysts was seen.

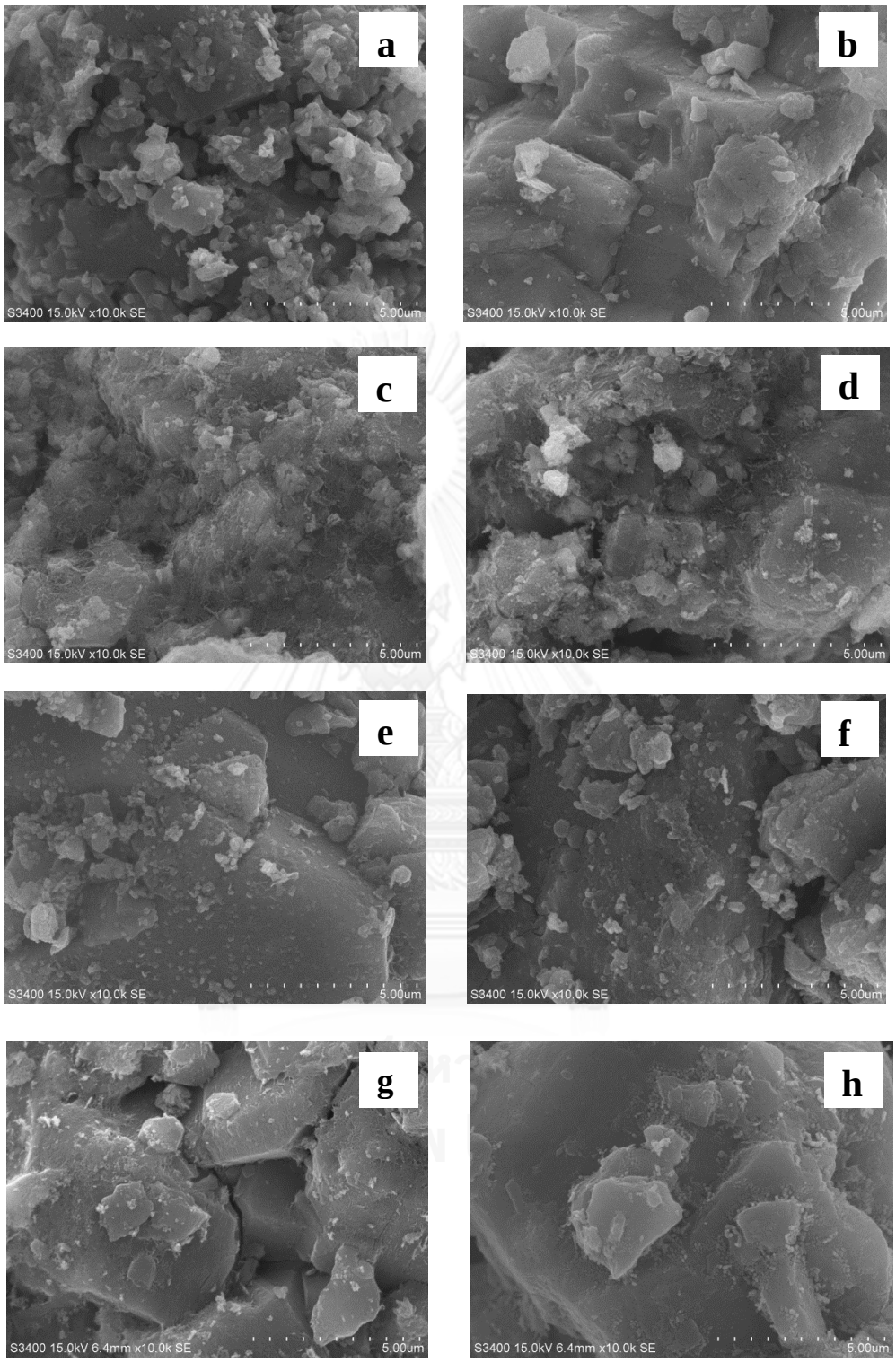

Figure 4.3 SEM images of all the catalysts. (a) Co/γ-Al_2O_3, (b) Co/γ-Al_2O_3_IWI, (c) 1CeCo/γ-Al_2O_3, (d) 1CuCo/γ-Al_2O_3, (e) 1KCo/γ-Al_2O_3, (f) 1MnCo/γ-Al_2O_3, (g) CeCo/γ-Al_2O_3, and (h) CuCo/γ-Al_2O_3

4.1.1.3 Nitrogen physisorption

Textural properties of the support and catalysts were measured by nitrogen physisorption. The BET surface area, pore volume, and pore size of the γ-Al_2O_3, monometallic, and bimetallic are listed in Table 4.2. The surface area of the support γ-Al_2O_3 formed by calcination of gibbsite at 650 °C was 126 m^2/g while its total pore volume and average pore size were equal to 0.23 cm^3/g, 4.8 nm, respectively. The significant decline in surface area, pore volume and average pore diameter of the monometallic Co/γ-Al_2O_3 prepared by incipient wetness impregnation as cobalt precursor solution was adsorbed in pores of γ-Al_2O_3, resulting in the formation of cobalt oxide within the pores. On the other hand, the once prepared by solid-state reaction had higher value than incipient wetness impregnation method suggesting that cobalt oxide particle appeared on the external surface of γ-Al_2O_3 support. The results are in agreement with the XRD analysis.

The Co/γ-Al_2O_3 promoted with 1.0 wt.% K, Mn, Cu, and Ce had BET surface area varied in the range of 119-134 m2/g in the order: 1MnCo > 1KCo > 1CeCo > 1CuCo > Co. For the same mole ratio of X:Co equal to 0.07 (X = Mn, Cu, and Ce) catalysts, the BET surface area varied in the range of 134-138 m2/g in the following order CeCo > CuCo > MnCo. Therefore, the increase in surface area, pore volume, and pore size after addition of second metal on Co/γ-Al2O3 catalysts by solid-state reaction indicated that the metal nanoparticles can disperse better than the monometallic.

Table 4.2 BET surface area, pore volume, and pore size

Catalysts	Surface area (m^2/g)	Total pore volume (cm^3/g)	Average pore size (nm)
γ-Al_2O_3	126	0.23	4.81
Co/γ-Al_2O_3	115	0.20	4.46
Co/γ-Al_2O_3-IWI	80	0.15	4.75
1CeCo/γ-Al_2O_3	121	0.19	3.88
1CuCo/γ-Al_2O_3	119	0.20	3.92
1KCo/γ-Al_2O_3	131	0.19	3.56
1MnCo/γ-Al_2O_3*	134	0.21	3.76
CeCo/γ-Al_2O_3*	138	0.22	3.87
CuCo/γ-Al_2O_3*	137	0.22	3.72

* The same mole ratio X:Co = 0.07 (X= Mn, Cu, and Ce)

4.1.1.4 Inductively coupled plasma (ICP)

ICP technique was used to detect that the metal contents of the catalysts compared to the targeted metal content of 15 wt.% Co, The result are shown in Table 4.3. The results indicated that the actual amount of cobalt for both solid-state reaction and incipient wetness impregnation method were slightly lower than the targeted amount. Additionally, the actual amount of cobalt for solid-state reaction appeared lower than another method as the incipient wetness impregnation used the cobalt precursor solution for prepared process, resulting in higher amount of deposited cobalt on the γ-Al_2O_3 support. **Table 4.3** ICP data of monometallic prepared solid-state reaction and incipient wetness impregnation method

Table 4.3 ICP data of monometallic prepared solid-state reaction and incipient wetness impregnation method

Catalysts	Loading Co	ICP
Co/γ-Al_2O_3	15	10
Co/γ-Al_2O_3_IWI	15	13

4.1.1.5 X-ray photon spectroscopy (XPS)

The elemental composition on the catalyst surface was examined by XPS and the results are shown in **Table 4.5**. In the literature, the various peaks of cobalt species were presented at 778.3 eV and 793.3 eV for Co^0, 780.4 eV, 795.8 eV for Co^{2+} and 778.5 eV and 794.2 eV for Co^{3+} [43].

The binding energy and atomic concentration of Co 2p, O 1s, Al 2s, Cu 2p, Ce 3d, K 2p, and Mn 2p are shown in **Table 4.5** while the literature data of various Co-containing compound are shown in **Table 4.5**. As shown in **Table 4.5**, the Co $2p_{3/2}$ XPS spectrum of Co/γ-Al_2O_3 catalyst prepared by incipient wetness impregnation showed major peak with B.E. values at 781.1 eV and the atomic ratio of Co/Al was equal to 0.23. The peak at 530.1 eV corresponded to the O 1s in Co_3O_4. The results suggested that the particles formed on the catalyst surface were Co_3O_4 [44]. On the other hand, the Co $2p_{3/2}$ peak of Co/γ-Al_2O_3 catalyst prepared by solid-state reaction was shifted toward higher binding energy (783.7 eV). It is suggested that the catalysts prepared by solid-state reaction gave significant higher interaction between support and cobalt species during calcination process. For the bimetallic catalysts, the XPS spectra of Cu 2p showed two major peaks at binding energies 934.6 and 936.7 eV corresponding to Cu^{2+} in CuO and $Cu(OH)_2$, respectively [45]. The

peaks of Ce 3d consisted of Ce $3d_{3/2}$ and Ce $3d_{5/2}$ species which had B.E. values of 883.9, 898.2 eV for Ce $3d_{5/2}$ and 902.8, 917.0 for Ce $3d_{3/2}$, corresponding to Ce^{4+} in CeO_2 [46]. The K $2p_{3/2}$ binding energy was at 284.9 eV which can be indicated to the potassium oxides [47]. The Mn $2p_{3/2}$ XPS peak was detected at B.E. values at 642.6 eV which can be attributed to Mn^{4+} in MnO_2 [48]. From **Table 4.5**, it is shown that the addition of K and Cu on Co/γ-Al_2O_3 catalysts apparently shifted the Co $2p_{3/2}$ peaks toward lower binding energy (782.9 and 783.0 eV, respectively) than the binding energy of Co_3O_4 (see Table 4.5). The addition of Mn and Ce on Co/γ-Al_2O_3 catalysts, the binding energy at 780.9 and 780.5 eV, respectively which can be clearly indicated Co_3O_4 on the catalysts surface. In addition, the atomic ration of Co/Al also increased from 0.19 to 0.30-0.90, suggesting more cobalt oxide were distributed on the surface of γ-Al_2O_3 support.

For the similar mole ratio of X:Co 0.07 catalysts, The peaks of Ce 3d composed of Ce $3d_{3/2}$ and Ce $3d_{5/2}$ species which was detected at B.E. values at 902.8, 917.08 eV for Ce $3d_{3/2}$ 83.9, 989.2 eV for Ce $3d_{5/2}$. The Cu 2p peak showed two major peaks with B.E. values at 923.0 and 933.4eV. The atomic of Co/Al also increased from 0.19 to 0.41-0.90; therefore, the addition of Mn, Ce, and Cu can increase amount cobalt oxide on the surface of γ-Al_2O_3 supports.

Table 4.4 XPS Data and characteristics of Cobalt-Containing Reference Materials.

Material	Binding energy of $Co2p_{3/2}$ (eV)	Reliability (eV)	Reference
Co	778.1	±0.1	[13]
CoO	780.1	±0.9	[13]
Co_3O_4	780.0	±0.7	[13]
$Co(OH)_2$	780.9	±0.2	[13]
CoO(OH)	780.1	NA	[50]
$Co(NO_3)_2$	781.9	NA	[13]
$CoAl_2O_4$	781.9	±0.5	[13]

Table 4.5 XPS data of monometallic and bimetallic catalysts.

Catalysts	B.E.(eV)			Second metal		Atomic ratio Co/Al	Atomic ratio X/Al
	Co $2p_{3/2}$	Al 2S	O 1S	Species	B.E. (eV)		
Co/γ-Al_2O_3	783.7	122.3	533.8	-	-	0.19	-
Co/γ-Al_2O_3_IWI	781.1	120.7	530.1	-	-	0.23	-
1CeCo/γ-Al_2O_3	780.5	119.7	531.1	Ce $3d_{5/2}$ Ce $3d_{3/2}$	883.9, 989.2 902.8, 917.0	0.30	0.22
1CuCo/γ-Al_2O_3	783.0	121.6	533.3	Cu $2p_{3/2}$	934.6, 936.7	0.45	0.12
1KCo/γ-Al_2O_3	782.9	121.2	533.2	K $2p_{3/2}$	284.9	0.39	0.07
1MnCo/γ-Al_2O_3*	780.9	119.2	530.6	Mn $2p_{3/2}$	642.6	0.67	0.07
CeCo/γ-Al_2O_3*	782.5	121.1	532.4	Ce $3d_{5/2}$ Ce $3d_{3/2}$	885.5, 890.7 910.0, 919.6	0.90	0.33
CuCo/γ-Al_2O_3*	782.6	121.4	533.1	Cu $2p_{3/2}$	923.0, 933.4	0.41	NA[(a)]

* The same mole ratio X:Co = 0.07 (X= Mn, Cu, and Ce)

[(a)] not avilable

4.1.1.6 Temperature program reduction (TPR)

H_2-TPR was used to study the reduction behavior and reducibility of the catalysts. The H_2-TPR profiles and reductions temperatures of the promoted and non-promoted catalysts are shown in **Figure 4.4** and **Figure 4.5**. There are three different cobalt species in the Co/γ-Al_2O_3: Co_3O_4 particles, Co^{2+} species and a spinel structure of $CoAl_2O_4$. The TPR profile of the supported cobalt oxide occurs in two reaction steps [1]:

First step: $Co_3O_4 + H_2 \longrightarrow 3CoO + H_2O$

Second step: $CoO + H_2 \longrightarrow Co + H_2O$

The TPR data shows that cobalt reducibility was affected by the addition of a second metal. However, TPR measurement was only used for qualitative information on cobalt reducibility but could not be used for quantitative of the proportion of cobalt metal phase in catalysts reduced in pure hydrogen. According to Sexton et al. [50], TPR reduction profile for Co_3O_4 typically contains a low-temperature peak at about 300 °C and a high-temperature peak about 500-700°C. The H_2-TPR profiles of non-promoted and 1wt.% K, Mn, Cu, and Ce promoted Co/γ-Al_2O_3 catalysts are shown in **Figure 4.5**. The TPR profile of alumina supported cobalt catalyst showed the first peak at 170 °C and the second peak at 400 °C, corresponding to the reduction of Co_3O_4 to Co^0. In addition, a small temperature peak below 300 °C was ascribed to the decomposition of $Co(NO_3)_2$ remaining after calcination at 650 °C or the reduction of CoO(OH) species [50]. From **Figure 4.4** the bimetallic catalysts exhibited different reduction profiles compared to the monometallic ones in which the reduction peaks of the bimetallic catalysts were

shifted toward higher temperature. In addition, 1MnCo/γ-Al_2O_3 catalyst the second peak was separated into two maximum temperatures (540 °C and 720 °C) owing presumably to the interaction of the cobalt surface species with the support. H_2 consumption and reducibility of all the catalysts were compiled in **Table 4.6**. It can be seen that addition of 1wt% second metal resulted in an increased reducibility which was higher (60%-86%) than the non-promoted Co/γ-Al_2O_3 catalyst (56%). According to these results, the addition of 1wt% promoters may increase strong interaction between metal and support which it is much stronger for smaller particles than for larger ones. For this result, it indicated that the TPR data conforms to the crystallite size from XRD analysis.

Regarding the same mole ratio of X:Co catalysts, **Figure 4.5** shows the H_2-TPR profile of these catalysts. For Ce and Cu promoted catalysts, the reduction peak shifted to lower temperature and also the reducibility were 38 and 34%, respectively. On the other hand, addition of Mn led to a shift toward higher temperature as well as increasing reducibility (75%). This result indicated that the addition of Mn improved the reduction of Co_3O_4 while opposite trend was found on Ce and Cu promoted ones. This may be due to possibly reasons that Cu and Ce blocked the active cobalt species, resulting in clearly decrease H_2 consumption and reducibility. Conclusively, promotion of Co/γ-Al_2O_3 with second metals may lead to the direct interaction between cobalt and promoters and formation of bimetallic cobalt-second metal particles which can occur during calcination process or during reduction of cobalt catalysts [53].

Table 4.6 H_2 consumption and % reducibility from TPR

Catalysts	H_2 consumption (μmole)	%reducibility
Co/γ-Al_2O_3	127.6	56
Co/γ-Al_2O_3_IWI	99.5	34
1CeCo/γ-Al_2O_3	135.7	68
1CuCo/γ-Al_2O_3	153.3	60
1KCo/γ-Al_2O_3	194.5	86
1MnCo/γ-Al_2O_3*	168.9	75
CeCo/γ-Al_2O_3*	85.5	38
CuCo/γ-Al_2O_3*	77.1	34

* The same mole ratio of X:Co = 0.07 (X= Mn, Cu, and Ce)

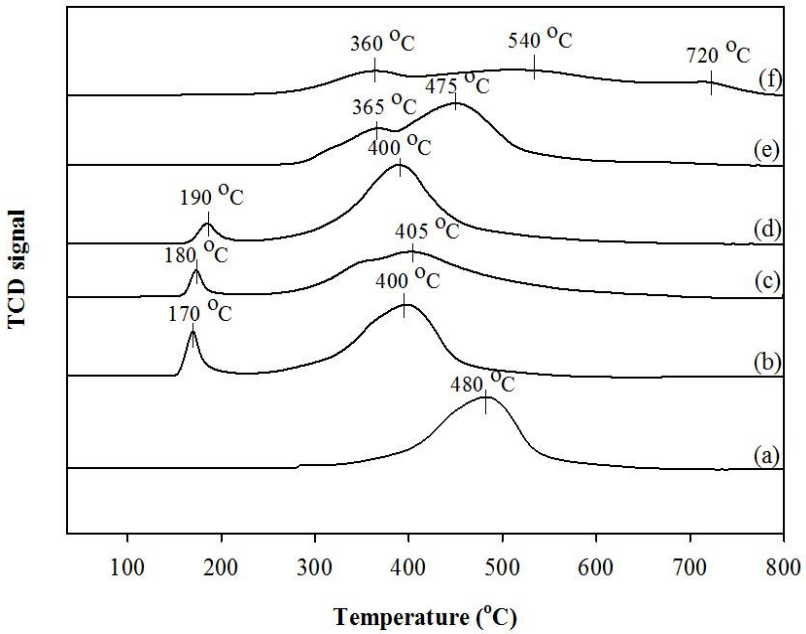

Figure 4.4 H_2-TPR profiles of non-promoted and 1wt.% promoted catalysts (a) Co/γ-Al_2O_3_IWI, (b) Co/γ-Al_2O_3, (c) 1CeCo/γ-Al_2O_3, (d) 1CuCo/γ-Al_2O_3, (e) 1KCo/γ-Al_2O_3, and (f) 1MnCo/γ-Al_2O_3.

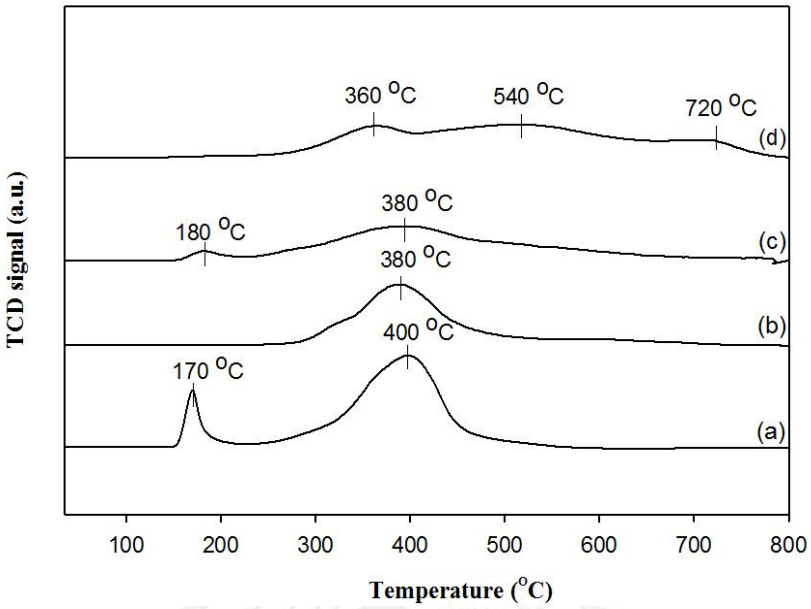

Figure 4.5 H_2-TPR profiles of of non-promoted and promoted catalysts , which have the same mole ratio X:Co = 0.07 (X= Mn, Cu, and Ce), (a) Co/γ-Al_2O_3, (b) CeCo/γ-Al_2O_3, (c) CuCo/γ-Al_2O_3, (d) MnCo/γ-Al_2O_3

4.1.1.7 Hydrogen chemisorption

Hydrogen chemisorption measurements were carried out to estimate H_2 uptake data, cobalt dispersion, and average cobalt crystallite size for all the catalysts after reduction at 350 °C for 3 h. The results are summarized in **Table 4.7**. The amounts of H_2 uptake for Co/γ-Al_2O_3 catalyst prepared by solid-state reaction were about 4.0 times more than that prepared by incipient wetness impregnation (Co/γ-Al_2O_3_IWI) catalysts. Although the cobalt oxides on Co/γ-Al_2O_3 prepared by solid-state reaction were large, all of them were easily reduced to metallic cobalt. Thus, a metallic crystallite size (12 nm) was smaller than cobalt oxide from XRD analysis. On the other hand, the metallic crystallite size of Co/γ-Al_2O_3_IWI (48 nm) was larger than cobalt oxide as all of them cannot reduced

to metallic cobalt, resulting in incorporated cobalt species. The addition of 1.0 wt.% promoters (K, Mn, Cu, and Ce) over Co/γ-Al_2O_3 catalysts, prepared by solid-state reaction led to an increase of the H_2 uptake and cobalt metal dispersion, except 1CuCo/γ-Al_2O_3, that the value was lower than the non-promoted one. In addition, the results can be observed that the addition of 1wt.% of promoters decreased cobalt metal crystallite size from 12 nm to 8-9 nm, except 1CuCo/γ-Al_2O_3 catalyst. The results indicated that the crystallite size of cobalt metallic obtained by reduction was smaller than cobalt oxide size, which was measured by XRD analysis, because cobalt particles were easily reconstructed and well dispersed during the reduction step. While 1CuCo/γ-Al_2O_3 catalyst, this may be due to two possibly reasons (i) a fraction of Cu tended to cover the rim of Co clusters and blocked Co surface sites [51] and/or (ii) Cu formed a highly dispersed Cu-aluminate [52] resulting in a decreased in the H_2 uptake.

Regarding the same mole ratio of X:Co catalysts, **Table 4.6** shows H_2 uptake data, cobalt dispersion, and average cobalt crystallite size. Conclusively, the addition of Mn led to an increase of the H_2 uptake and cobalt metal dispersion while opposite trend was found on Ce and Cu promoted ones. The TPR results suggest that addition of promoter increased the strongly interacting cobalt oxide crystallites with support; however cobalt dispersion was enhanced.

Table 4.7 H_2 uptake data, cobalt dispersion, and average cobalt crystallite size of monometallic and bimetallic.

Catalysts	Cobalt dispersion	H_2 uptakes ($x10^{-18}$ molecules/g.cat)	Co^0 crystallite size
Co/γ-Al_2O_3	8.4	17.24	12
Co/γ-Al_2O_3_IWI	2.1	5.55	48
1CeCo/γ-Al_2O_3	13.2	26.89	8
1CuCo/γ-Al_2O_3	7.5	15.41	13
1KCo/γ-Al_2O_3	11.5	23.48	9
1MnCo/γ-Al_2O_3*	11.1	22.74	9
CeCo/γ-Al_2O_3*	5.6	11.42	18
CuCo/γ-Al_2O_3*	4.3	8.74	23

* The same mole ratio of X:Co = 0.07 (X= Mn, Cu, and Ce)

4.1.2 The catalytic activity in carbon dioxide hydrogenation

The reaction was carried out in the carbon dioxide hydrogenation to determine the catalytic activity. Prior to the reaction test, the catalyst was reduced at 350 °C in flowing H_2 for 3 h. And then, the catalysts were cooled to 270 °C in flowing N_2. After purging with the pre-mixed gas, the reactant gases consisting of H_2/CO_2 were gradually introduced to the reactor.

The CO_2 hydrogenation was used to measure the overall activity to determine the catalytic properties of catalyst samples. Carbon dioxide hydrogenation of all the catalysts at 270 °C, the selectivity for hydrocarbon compound was 100%.

The detected hydrocarbon compound was only methane and water was also noticed during carbon dioxide hydrogenation reaction**.** The results showed that the CO_2 conversion of Co/γ-Al_2O_3 (39%) catalyst was higher than Co/γ-Al_2O_3_IWI (18%) catalyst. The catalytic properties were obviously related to the TPR and H_2 chemisorption results as mentioned above. From **Figure 4.6**, it is shown that the CO_2 conversion for all the promoted catalysts was higher (47-66%) than the non-promoted Co/γ-Al_2O_3 catalyst (14.5%), except 1CuCo/γ-Al_2O_3 that exhibited lower CO_2 conversions (24%). From **Table 4.8**, it can be seen that the promoted catalysts showed the reaction rate in the order: 1KCo > 1MnCo > 1CeCo > Co > 1CuCo.

For 1KCo/γ-Al_2O_3 catalyst, it showed the highest both the CO_2 conversion and the reaction rate. The results suggested that the addition of K, Mn, and Ce on Co/γ-Al_2O_3 can increase cobalt active site and enhance reducibility which was determined by H_2 chemisorption and H_2-TPR, respectively. A previous report [54] been suggested that the addition of K was led to structure promoter's effect resulting in an increase of apparent activation energy of reduction process of cobalt oxide. For the Mn promoter the catalytic activity was also improved resulting from an increase of the Co dispersion. It is proposed in a previous report [55] that the addition of Mn led to aiding in an appreciable increase in metallic Co, influenced the catalytic activity by an electronic effect. On the other hand, the addition of Cu decreased both the CO_2 conversion and the reaction rate due to a declined cobalt active site and reducibility. It had possibly reasons (i) a fraction of Cu blocked Co surface sites [51] and/or (ii) Cu formed a highly dispersed Cu-aluminate [52]. The results obtained for promoted catalysts, which were specified the same mole ratio of

X:Co = 0.07 were illustrated in **Figure 4.7** and **Table 4.8**. Similarity, the result of 1wt% promoted catalysts was previously described.

Table 4.8 Catalytic activity of CO_2 hydrogenation of the all catalysts

Catalysts	CO_2 conversion (%)	Reaction rate ($\times 10^2$ $g_{CH2} \cdot g_{cat}^{-1} \cdot h^{-1}$)
Co/γ-Al_2O_3	39	29.2
Co/ γ-Al_2O_3_IWI	18	13.7
1CeCo/ γ-Al_2O_3	47	35.0
1CuCo/ γ-Al_2O_3	24	17.8
1KCo/ γ-Al_2O_3	66	41.5
1MnCo/ γ-Al_2O_3*	55	49.3
CeCo/ γ-Al_2O_3*	39	29.3
CuCo/ γ-Al_2O_3*	29	22.1

* The same mole ratio of X:Co = 0.07 (X= Mn, Cu, and Ce)

Reaction condition: 270 C, 1 atm, H_2/CO_2 = 10/1. The conversion and reaction rate based on amount of CH_4

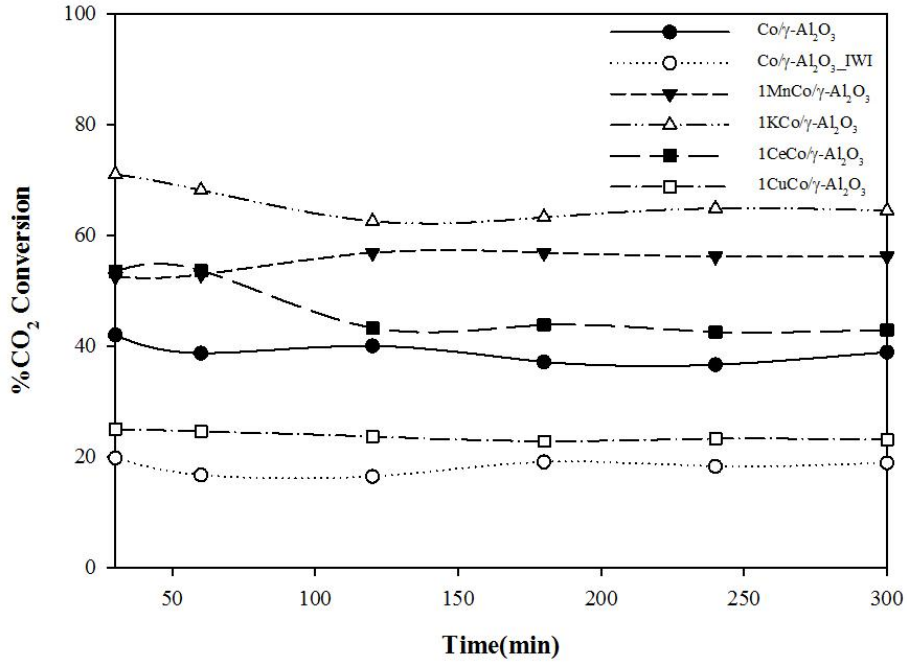

Figure 4.6 Stability test results of non-promoted and 1wt.% promoted catalysts at 443 K, 1 atm, H_2/CO_2 ratio 10, flow rate 21.3 cm^3/min.

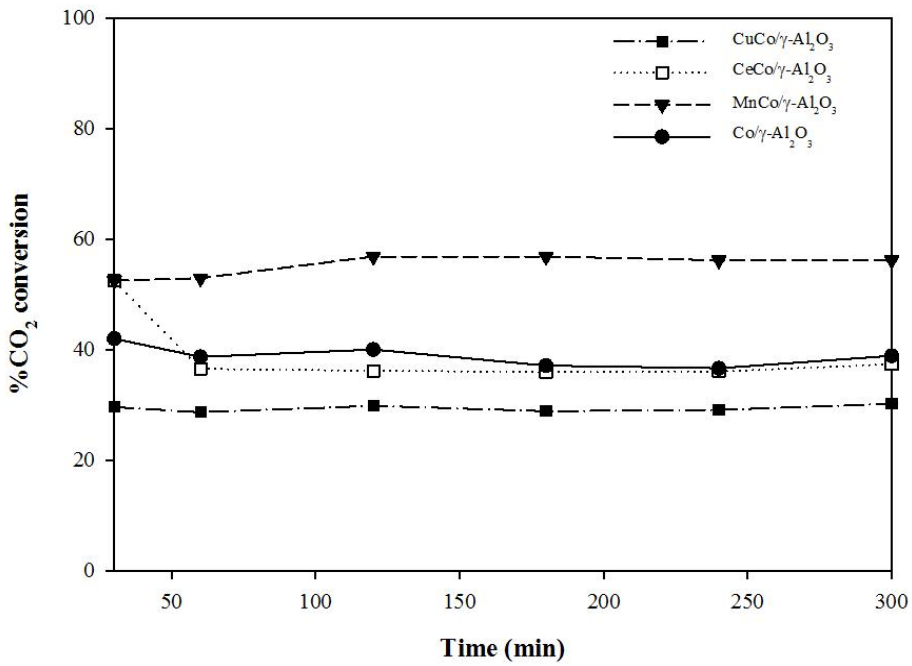

Figure 4.7 Stability test results of non-promoted and promoted catalysts, which had the same mole ratio of X:Co = 0.07 (X= Mn, Cu, and Ce) at 443 K, 1 atm, H_2/CO_2 ratio 10, flow rate 21.3 cm^3/min.

4.2 Effect of difference amounts of the selected promoter on the properties of Co/γ-Al_2O_3 catalysts

4.2.1 Characterization of Catalysts

4.2.1.1 X-ray diffraction (XRD)

The XRD patterns of the different amounts of K and Mn promoted Co/γ-Al_2O_3 catalysts after calcination which were prepared by solid-state reaction and incipient wetness impregnation method are shown in **Figure 4.8** and **Figure 4.9** respectively**.** The XRD patterns were recorded over a 2θ range of 10°–80°. The diffraction patterns of the formation of a Co_3O_4 phase appeared at 2θ 18.9°, 31.5°, 37.0°, 44.9°, 55.9, 59.7° and 65.2° [14] in the all catalysts. The peaks at 2θ values of 37°, 43°, 46°, and 67° [4] corresponded to that of γ-Al_2O_3. From **Figure 4.8**, it can be seen that different amounts of K (0.5-2.0wt.%) promoted Co/γ-Al_2O_3 exhibited similar diffraction patterns. Likewise, average Co_3O_4 crystallite sizes, which were compiled in **Table 4.9** were estimated ranging from 42 to 47 nm and were slightly larger than the non-promoted (28 nm). In term of the different amount of promoted Mn (0.5-2.0wt.%) in **Figure 4.9**, it was found that intensity of diffraction peak decreased significantly with increasing content of Mn. Similarly, average Co_3O_4 crystallite size of the all these catalysts are shown **Table 4.9** and declined in the following order 0.5MnCo > 1MnCo > 2MnCo and all of them were smaller than non-promoted one (28 nm). It clearly seen that the addition of small amount of Mn on Co/γ-Al_2O_3 catalysts changed the average Co_3O_4 particle size due to higher dispersion of cobalt species on the catalysts surface. In addition, the XRD patterns of 1KCo/γ-Al_2O_3 and 1MnCo/γ-Al_2O_3 prepared incipient wetness impregnation method showed lower intensity than the ones prepared by solid state reaction, as a consequence average

Co_3O_4 crystallite size decreased from 42 to 14 nm and 19 to 9, respectively. This may be due to cobalt loading which can enter some pores of γ-Al_2O_3 support after incipient wetness impregnation which was also confirmed by nitrogen physisorption.

Table 4.9 Average Co_3O_4 crystallite size of a series of K and Mn promoted Co/γ-Al_2O_3 catalysts

Catalysts	Average Co_3O_4 crystallite size from XRD (nm)
Co/γ-Al_2O_3	38
0.5KCo/γ-Al_2O_3	42
1.0KCo/γ-Al_2O_3	42
2.0KCo/γ-Al_2O_3	47
1.0KCo/γ-Al_2O_3 _IWI	14
0.5MnCo/γ-Al_2O_3	29
1.0MnCo/γ-Al_2O_3	19
2.0MnCo/γ-Al_2O_3	14
1.0MnCo/γ-Al_2O_3_IWI	9

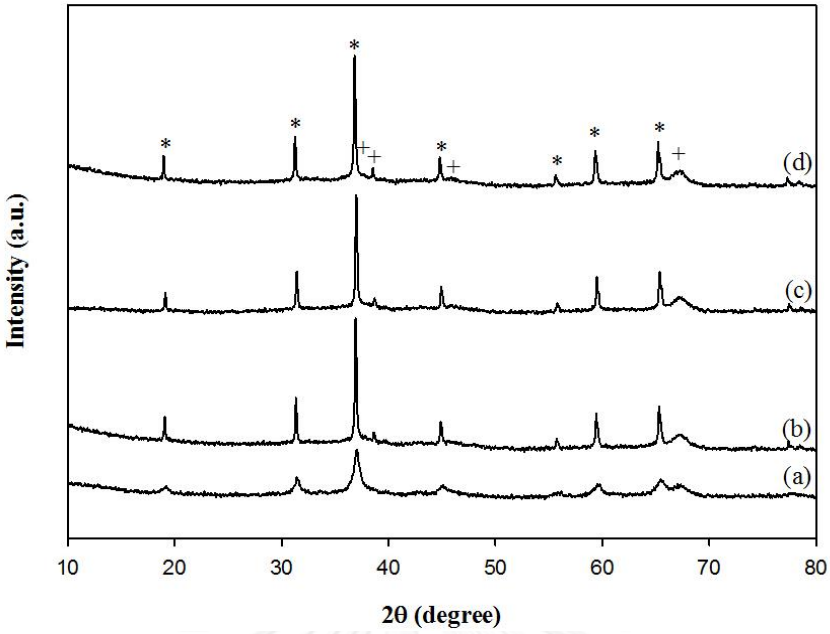

Figure 4.8 XRD patterns of difference amount of K promoted Co/γ-Al_2O_3 catalysts after calcination in air at 650 °C for 5 h. (a) 1KCo/γ-Al_2O_3_IWI, (b) 0.5KCo/γ-Al_2O_3, (c) 1KCo/γ-Al_2O_3, and (d) 2KCo/γ-Al_2O_3 (*) indicates the Co_3O_4 phase and (+) indicates the γ-Al_2O_3 phase from support.

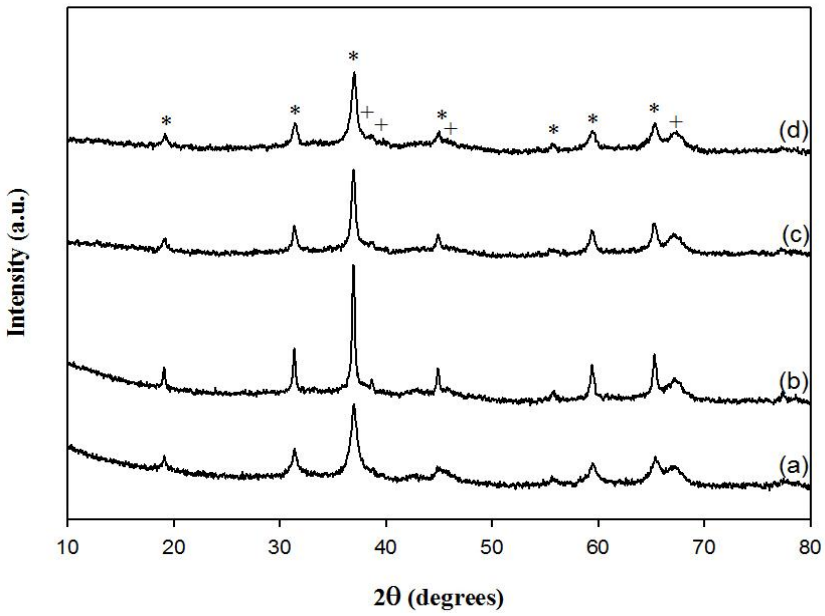

Figure 4.9 XRD patterns of difference amount of Mn promoted Co/γ-Al_2O_3 catalysts after calcination in air at 650 °C for 5 h. (a) 1MnCo/γ-Al_2O_3_IWI, (b) 0.5MnCo/γ-Al_2O_3, (c) 1MnCo/γ-Al_2O_3, and (d) 2MnCo/γ-Al_2O_3 , (*) indicates the Co_3O_4 phase and (+) indicates the γ-Al_2O_3 phase from support.

4.2.1.2 Scanning Electron Microscope (SEM)

The morphology and distribution of particles over support was determined from SEM analysis. **Figure 4.10** exhibits the representative SEM images of the K and Mn promoted Co/γ-Al_2O_3 catalysts. From SEM result, the cobalt oxide particles deposited on γ-Al_2O_3 support were highly dispersed with increasing K and Mn promoted catalysts ranging 0.5-2.0 wt.% as can be seen **Figure 4.10**. Comparing the catalysts prepared by difference method, the incipient wetness impregnation methods gave smoother surface and smaller particles than the solid-state reaction.

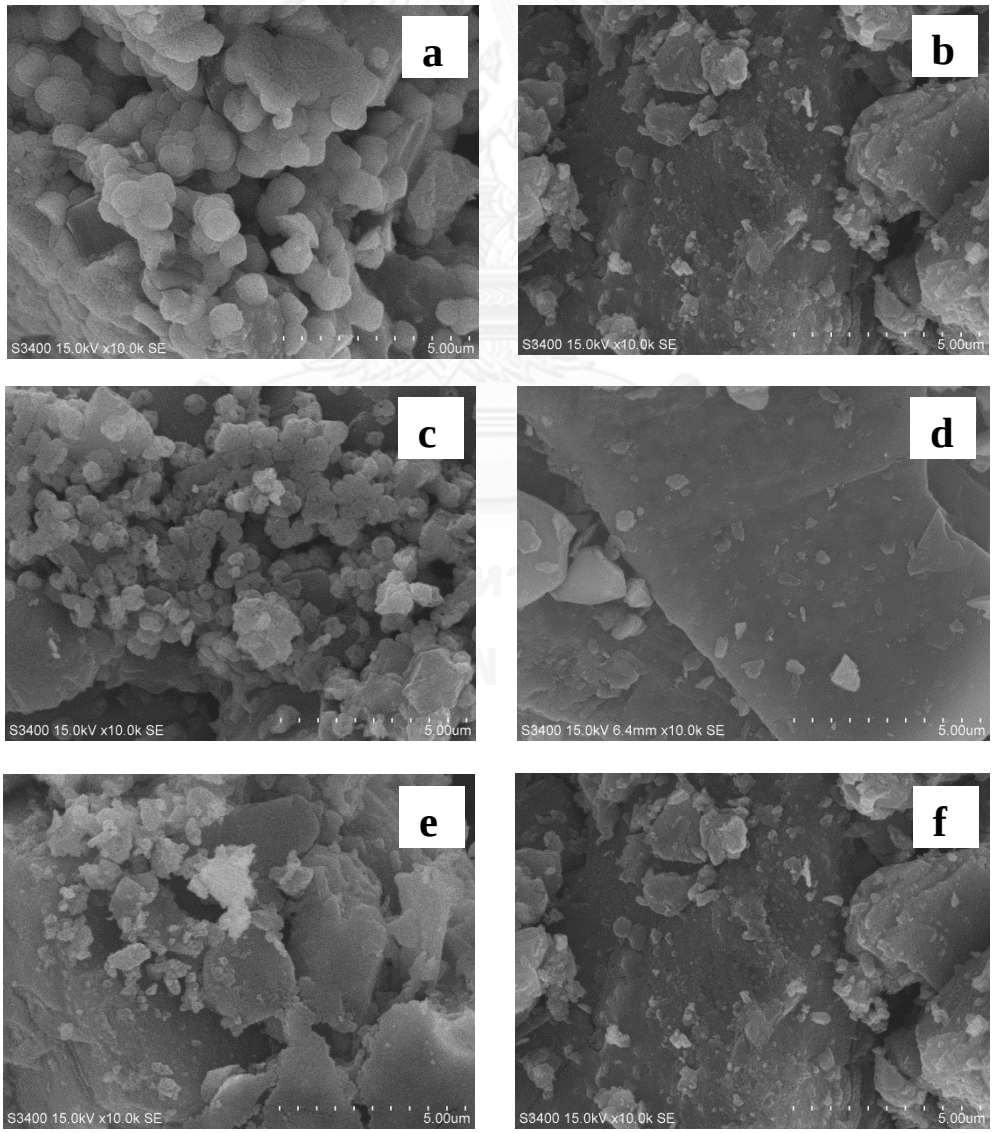

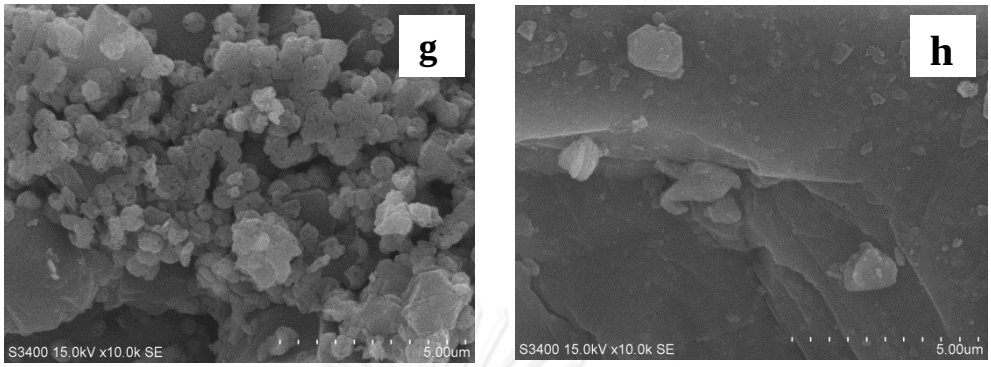

Figure 4.10 SEM images of all the catalysts. (a) 0.5KCo/γ-Al_2O_3, (b) 1KCo/γ-Al_2O_3, (c) 2KCo/γ-Al_2O_3, (d) 1KCo/γ-Al_2O_3_IWI, (e) 0.5MnCo/γ-Al_2O_3, (f) 1MnCo/γ-Al_2O_3, (g) 2MnCo/γ-Al_2O_3, (h) 1MnCo/γ-Al_2O_3_IWI

4.2.1.3 Nitrogen physisorption

The BET surface area, pore volume, and pore size of the different amounts of Mn and K promoted catalysts prepared by solid-state reaction and incipient wetness impregnation method by nitrogen physisorption are listed in **Table 4.9**. All of the K and Mn promoted catalysts prepared by solid-state reaction exhibited higher surface area than non-promoted. Among the three Mn promoted catalysts, 1MnCo/γ-Al_2O_3 catalyst gave the highest surface area. Increasing of the Mn loading had little contribution to the surface area, total pore volume and pore size of the catalysts (see **Table 4.9**). For the various K loadings, 1KCo/γ-Al_2O_3 catalyst gave the highest surface area (131 m^2/g), and total pore volume (0.19 cm^3/g). The pore size was not increased with increasing K loading. It was observed that 1KCo/γ-Al_2O_3 had the smallest pore size (3.56 nm). In both types of promoted catalysts, 1Mn and 1K seemed to be highly dispersed over the /γ-Al_2O_3 support. In addition, surface area and pore volume for 1MnCo/γ-Al_2O_3 and 1KCo/γ-Al_2O_3 prepared by solid-state

reaction were higher than the incipient wetness impregnation while its pore size was smaller. This result may be probably because the metal loading accessed some pores of γ-Al_2O_3 after impregnation, bringing about the decrease of surface area, pore volume of the catalysts.

Table 4.10 BET surface area, pore volume, and pore size of a series of K and Mn promoted Co/γ-Al_2O_3 catalysts

Catalysts	surface area (m^2/g)	pore volume (cm^3/g)	pore size (nm)
Co/γ-Al_2O_3	115	0.20	4.46
0.5MnCo/γ-Al_2O_3	128	0.20	3.63
1MnCo/γ-Al_2O_3	134	0.21	3.76
2MnCo/γ-Al_2O_3	127	0.20	3.94
1MnCo/γ-Al_2O_3_IWI	85	0.16	4.76
0.5KCo/γ-Al_2O_3	128	0.19	3.63
1KCo/γ-Al_2O_3	131	0.19	3.56
2KCo/γ-Al_2O_3	116	0.18	3.67
1KCo/γ-Al_2O_3_IWI	86	0.15	4.69

4.1.1.4 X-ray photon spectroscopy (XPS)

XPS analysis was used to investigate the surface composition of the catalysts. In the literature, the various peaks of cobalt species were presented at 778.3 eV and 793.3 eV for Co^0, 780.4 eV, 795.8 eV for Co^{2+} and 778.5 eV and 794.2 eV for Co^{3+} [43].

The Co $2p_{3/2}$, O 1s, Al 2s, K 2p, and Mn 2p were compiled in **Table 4.10**. The Co $2p_{3/2}$ peak of Co/γ-Al_2O_3 catalyst prepared by solid-state reaction was shifted toward higher binding energy (783.7 eV) and the atomic ratio of Co/Al was equal to 0.19. An increase of atomic ratio of Co/Al was found all on the various amounts of K and Mn, which were prepared by solid-state reaction, except 2KCo/γ-Al_2O_3. It is indicated that higher amount of cobalt were distributed on the surface of γ-Al_2O_3 support. For a series of K loading on Co/γ-Al_2O_3 catalysts, the Co $2p_{3/2}$ XPS spectra of the three catalysts were shifted toward higher binding energy but for the addition of 2wt.%K on Co/γ-Al_2O_3 catalysts, binding energy at 782.5 eV was observed, which decreased from 1wt.%K. It can be suggested that increase of K loading led to higher interaction between cobalt and support while opposite trend was found on excess addition of 2wt.%K. Moreover, atomic ratios of Co/Al were ranging from 0.11 to 0.39. As for a series of Mn loading on Co/γ-Al_2O_3 catalysts, changes of binding energy of Co $2p_{3/2}$ were observed and Co/Al ratios increased from 0.19 to 0.67. The results indicated that the Co/Al ratio reflected more cobalt species on external surface of γ-Al_2O_3 support achieved values 0.39 for 1KCo/γ-Al_2O_3 and 0.67 for 1MnCo/γ-Al_2O_3 catalyst. In addition, the 1KCo/γ-Al_2O_3 and 1MnCo/γ-Al_2O_3 catalysts prepared by solid-state reaction had higher Co/Al ratio compared to the ones prepared by incipient wetness impregnation method.

Table 4.11 XPS data of a series of K and Mn promoted Co/γ-Al_2O_3 catalysts

Catalysts	B.E.(eV)				Second metal		Atomic ratio	Atomic ratio
	Co 2p		Al 2S	O 1S	Species	B.E. (eV)	Co/Al	X/Al
	$2p_{1/2}$	$2p_{3/2}$						
0.5KCo/g-Al_2O_3	798.0	782.3	121.7	533.1		285.0	0.24	1.27
1.0KCo/g-Al_2O_3	797.6	782.9	121.2	533.2	K $2p_{3/2}$	284.9	0.39	0.16
2.0KCo/g-Al_2O_3	797.5	782.5	121.0	533.2		285.5	0.11	0.57
1.0KCo/g-Al_2O_3 _IWI	793.7	783.2	121.0	533.5		285.1	0.19	0.36
0.5MnCo/g-Al_2O_3	797.1	781.8	120.4	532.2		642.6	0.51	0.02
1.0MnCo/g-Al_2O_3	796.1	780.9	119.2	530.6	Mn $2p_{3/2}$	642.6	0.67	0.07
2.0MnCo/g-Al_2O_3	796.4	781.0	118.7	530.3		642.0	0.49	0.13
1.0MnCo/g-Al_2O_3_IWI	799.3	783.4	121.0	533.5		646.7	0.22	0.02

4.2.1.5 Temperature program reduction (TPR)

TPR was used study the reduction behavior and reducibility of the catalysts. The H_2-TPR profiles and reduction temperatures of the different amounts of K and Mn promoted Co/γ-Al_2O_3 catalysts which were prepared by solid-state reaction and incipient wetness impregnation method are shown in **Figure 4.11** and **Figure 4.12**, respectively**.** There are three different cobalt species in the Co/γ-Al_2O_3: Co_3O_4 particles, Co^{2+} species and a spinel structure of $CoAl_2O_4$. The TPR profile of the supported cobalt oxide occurs in two reaction steps [1]:

First step: $Co_3O_4 + H_2 \longrightarrow 3CoO + H_2O$

Second step: $CoO + H_2 \longrightarrow Co + H_2O$

From **Figure 4.11,** the Co/γ-Al_2O_3 catalyst showed the first peak at 170 °C and the second peak at 400 °C, corresponding to the reduction of Co_3O_4 to Co^0. It can be clearly seen that the reduction temperature was lower than all promoted catalysts. For 0.5KCo/γ-Al_2O_3 catalyst, it exhibited the first peak at 180 °C and the second peak at 430 °C, attributing to the reduction of Co_3O_4 to Co^0. Moreover, a small peak below 300 °C was assigned to the decomposition of $Co(NO_3)_2$ remaining after calcination at 650 °C or the reduction of CoO(OH) species [50]. They were not affected by increasing promoter loading of K (1.0 and 2.0 wt%), but the two reduction peaks were shifted toward higher temperature and created their overlapping, as simultaneously generated two reduction step: Co_3O_4 to CoO and CoO to Co^0 and cobalt oxide was better distributed. Figure 4.12 presents H_2-TPR pattern of the different amount of Mn promoted Co/γ-Al_2O_3 catalysts. The 0.5MnCo/γ-Al_2O_3 displayed the first peak at 360 °C and the second peak at 460 °C whereas the

reduction peaks of 1MnCo/γ-Al_2O_3 and 2MnCo/γ-Al_2O_3 were shifted toward higher temperature and became broaden as cobalt particles may be dispersed better. The average crystallite size of cobalt metals were calculated from H_2 chemisorption results. Furthermore, it can be seen that the reducibility from Table 4.12 slightly increased as amount of promoters were added to catalysts ranged from 66 to 86% for the promoted K and ranged from 62 to 76% for promoted Mn. It is suggested that a series of K and Mn loading led to interaction of metal and support.

Comparing the catalysts prepared by different methods, **Figure 4.11** (c) and (e) indicated that 1KCo/γ-Al_2O_3 prepared by solid-state reaction exhibited overlapped reduction peaks at 365 °C and 450 °C, while the reduction peaks of 1KCo/γ-Al_2O_3 prepared by incipient wetness impregnation method were shifted toward higher temperature (450 °C, 600°C) while the reducibility decreased from 86 to 51%, respectively. Likewise, the TPR profiles of Mn promoted Co/γ-Al_2O_3 prepared by two different methods as 1MnCo/γ-Al_2O_3 prepared by solid-state reaction exhibited overlapped the reduction peaks at 360 °C and 460 °C, whereas the reduction peaks of 1MnCo/γ-Al_2O_3 prepared by incipient wetness impregnation method were shifted toward higher temperature (520 °C, 670°C) and the reducibility declined from 75 to 40%, respectively.

Table 4.12 H_2 consumption and reducibility of a series of K and Mn promoted Co/γ-Al_2O_3 catalysts

Catalysts	H_2 consumption (μmole/g.cat)	%reducibility
Co/γ-Al_2O_3	127.6	56
0.5KCo/γ-Al_2O_3	149.2	66
1.0KCo/γ-Al_2O_3	194.5	80
2.0KCo/γ-Al_2O_3	194.7	86
1.0KCo/γ-Al_2O_3_IWI	149.6	51
0.5MnCo/γ-Al_2O_3	139.8	62
1.0MnCo/γ-Al_2O_3	168.9	75
2.0MnCo/γ-Al_2O_3	171.6	76
1.0MnCo/γ-Al_2O_3_IWI	117.1	40

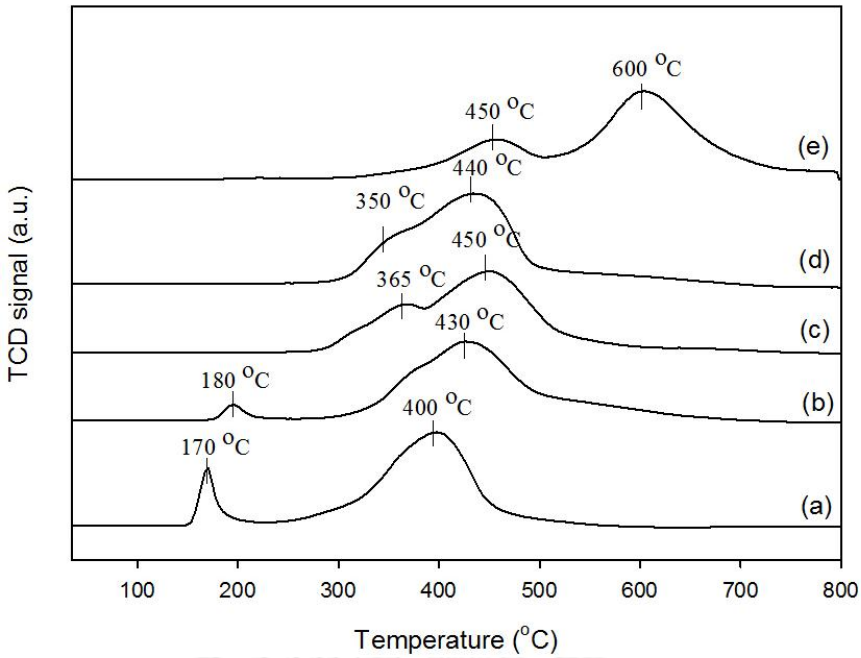

Figure 4.11 H_2-TPR profile of difference amount of K promoted Co/γ-Al_2O_3. (a) Co/γ-Al_2O_3, (b) 0.5KCo/γ-Al_2O_3, (c) 1KCo/γ-Al_2O_3, (d) 2KCo/γ-Al_2O_3, and (e) 1KCo/γ-Al_2O_3_IWI

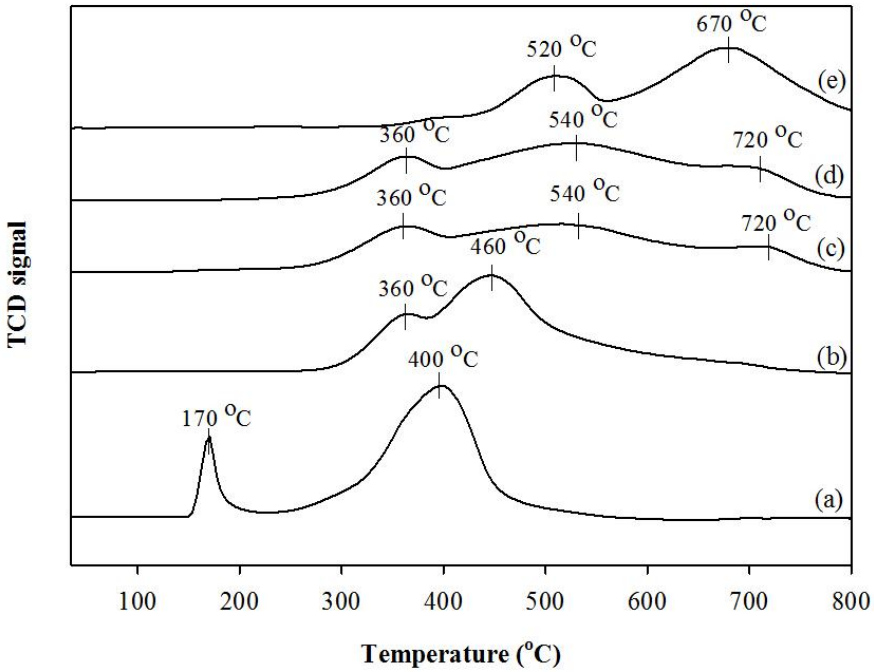

Figure 4.12 H_2-TPR profile of difference amount of Mn promoted Co/γ-Al_2O_3 catalysts. (a) Co/γ-Al_2O_3, (b) 0.5MnCo/γ-Al_2O_3, (bc) 1MnCo/γ-Al_2O_3, (d) 2MnCo/γ-Al_2O_3, and (e) 1MnCo/γ-Al_2O_3_IIWI

4.2.1.6 Hydrogen chemisorption

Chemisorption of hydrogen on the reduced catalysts was used to estimate dispersion of cobalt metal particle and average cobalt metal size for all the catalysts after reduction at 350 °C for 3 h. The results are shown in **Table 4.13**. The results demonstrate a little decrease of H_2 uptake and cobalt dispersion when the Co/γ-Al_2O_3 catalyst were promoted by different amounts of K ranging 0.5-2.0 wt.% while crystallite size of cobalt metal slightly increased from 7 nm to 11 nm. These trends are illustrated in **Table 4.13**. The addition of different amount of Mn (0.5-2.0 wt.%) resulted in the decline in hydrogen chemisorption. Adding K and Mn increased strongly interacting cobalt oxide particles; however, it was more difficult to reduce than corresponding bulk cobalt oxides. High reduction temperatures which required to create the active metal phase led to poor metal dispersion. A comparison of the catalysts prepared by different method revealed that for 1KCo/γ-Al_2O_3 and 1MnCo/ γ-Al_2O_3 prepared with incipient wetness impregnation method had lower cobalt dispersion than solid-state reaction. This may be attributed to very strong interaction of cobalt oxide crystallites for the ones prepared by incipient wetness impregnation which was confirm by TPR analysis.

Table 4.13 H_2 uptake data, cobalt dispersion, and average cobalt crystallite size of different amount of K and Mn promoted catalysts.

Catalysts	Cobalt dispersion	H_2 uptake ($x10^{-18}$ molecules/g.cat)	Crystallite size of Co^0
Co/γ-Al_2O_3	8.4	17.24	12
0.5KCo/γ-Al_2O_3	13.9	28.42	7
1KCo/γ-Al_2O_3	11.5	23.48	9
2KCo/γ-Al_2O_3	9.1	18.57	11
1KCo/γ-Al_2O_3_IWI	10.7	28.46	9
0.5MnCo/γ-Al_2O_3	13.6	27.81	7
1MnCo/γ-Al_2O_3	11.1	22.74	9
2MnCo/γ-Al_2O_3	5.8	11.94	17
1MnCo/γ-Al_2O_3_IWI	9.1	24.18	11

4.2.2 *The catalytic activity in carbon dioxide hydrogenation*

The reaction was carried out in carbon dioxide hydrogenation to determine the catalytic activity. Prior to the reaction test, the catalyst was reduced at 350 °C in flowing H_2 for 3 h. And then, the catalysts were cooled to 270 °C in flowing N_2. After purging with the pre-mixed gas, the reactant gases consisting of H_2/CO_2 were gradually introduced to the reactor.

The CO_2 hydrogenation was used to measure the overall activity to determine the catalytic properties of catalyst samples. A series of K and Mn

promoted Co/γ-Al_2O_3 catalysts with varying promoter from 0.5 to 2.0 wt.% prepared solid-state reaction and incipient wetness impregnation method were investigated by carbon dioxide hydrogenation reaction. The reaction was carried out at 270°C and 1 atm. Carbon dioxide hydrogenation of all the catalysts under these conditions, the selectivity for hydrocarbon compound was 100%. The detected hydrocarbon compound was only methane and water was observed during carbon dioxide hydrogenation reaction. From **Figure 4.13** and **Figure 4.14,** the CO_2 conversion varied with different amounts of K and Mn loading on Co/γ-Al_2O_3 catalysts. **Table 4.14**, the addition of K and Mn loading has an important effect on CO_2 conversion and reaction rate. The CO_2 conversion increased rapidly from 55% to 71% for the addition of K loading and increased slightly from 45% to 57% for the addition of Mn loading from 0.5 to 2.0 wt.%. Furthermore, it can be seen that reaction rate of all promoted catalysts showed in the order: 2KCo > 1KCo > 0.5KCo and 2MnCo > 1MnCo ≈ 0.5MnCo. The 1KCo/γ-Al_2O_3 and 1MnCo/γ-Al_2O_3 catalyst presented that all of them were optimum concentration of promoters because excess concentration (2wt.%) can only increase slightly CO_2 conversion and reaction rate. It is clear that a suitable amount of these promoters improved catalytic activity, increased surface area, enhanced reducibility and H_2 uptake.

For comparison of preparation methods between solid-state reaction and incipient wetness impregnation method for 1KCo/γ-Al_2O_3 and 1MnCo/γ-Al_2O_3, it was found that the catalysts prepared by solid-state reaction had higher reaction rate than the ones prepared by impregnation method. It may because impregnation

method led to the decrease of surface area and H_2 uptake, and excess strongly interacting cobalt metal.

Table 4.14 Effect of a series of K and Mn promoted Co/γ-Al_2O_3 catalysts on CO_2 conversion and CH_4 formation.

Catalysts	CO_2 conversion (%)	Reaction rate ($\times 10^2$ $g_{CH2} \cdot g_{cat}^{-1} \cdot h^{-1}$)
Co/γ-Al_2O_3	39	29.2
0.5KCo/γ-Al_2O_3	55	35.5
1KCo/γ-Al_2O_3	66	41.5
2KCo/γ-Al_2O_3	71	48.3
1KCo/γ-Al_2O_3_IWI	55	36.1
0.5MnCo/γ-Al_2O_3	45	41.3
1MnCo/γ-Al_2O_3	55	49.3
2MnCo/γ-Al_2O_3	57	53.7
1MnCo/γ-Al_2O_3_IWI	47	41.0

Reaction condition: 270 C, 1 atm, H_2/CO_2 = 10/1. The conversion and reaction rate based on amount of CH_4

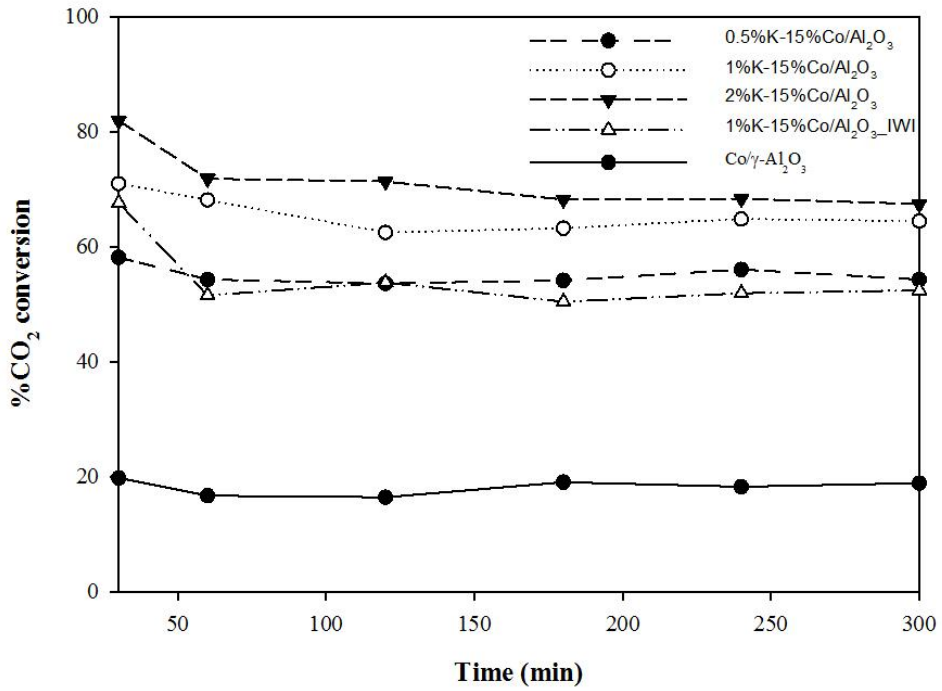

Figure 4.13 Effect of a series of K promoted Co/γ-Al_2O_3 catalysts on CO_2 conversion

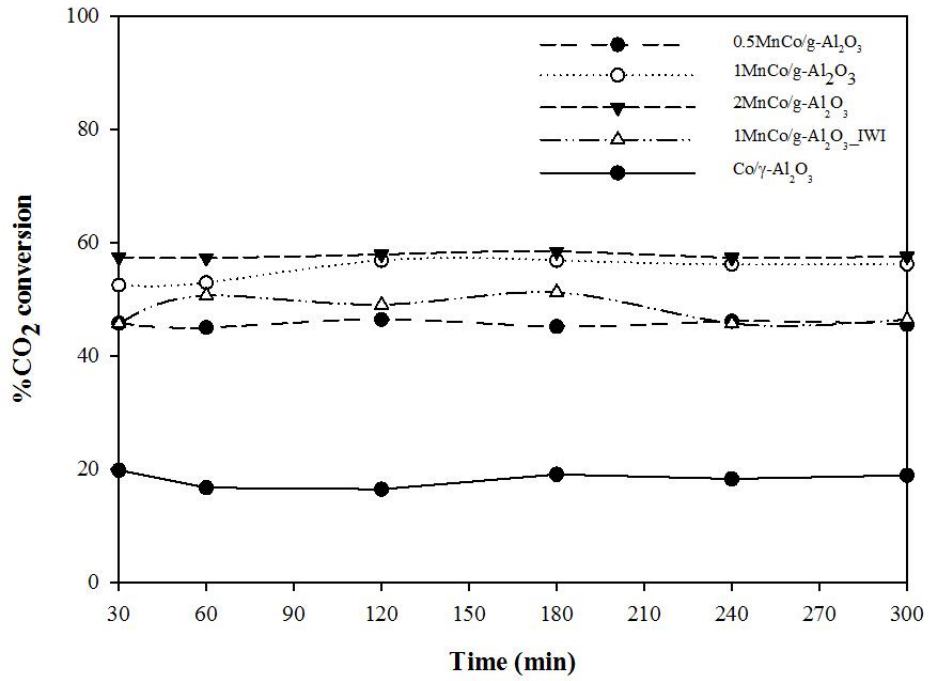

Figure 4.14 Effect of a series of Mn promoted Co/γ-Al_2O_3 catalysts on CO_2 conversion

CHAPTER V

CONCLUSIONS AND RECOMMENDATIONS

5.1 Conclusions

In this study, the effect of the different promoters including K, Mn, Cu, and Ce on the characteristics and catalytic properties of Co/γ-Al_2O_3 catalysts prepared by solid-state reaction in the carbon dioxide hydrogenation was investigated. CO_2 conversion for Co/γ-Al_2O_3 catalyst prepared by solid-state reaction was about 117% of prepared by incipient wetness impregnation (Co/γ-Al_2O_3_IWI) catalysts. The addition of K and Mn (1 wt.% or mole ratio of X/Co 0.07) during solid-state reaction of Co/γ-Al_2O_3 resulted in an enhanced catalytic performance in the CO_2 hydrogenation reaction due to higher Co dispersion and higher reducibility of Co_3O_4 crystallites. Compered to catalysts prepared by the conventional incipient wetness impregnation, all the solid-state catalysts exhibited much higher CO_2 conversion with 100% CH_4 selectivity.

A series of Co/γ-Al_2O_3 catalysts were also prepared with various amounts of K and Mn loading (0.5-2.0 wt.%) by solid-state reaction and incipient wetness impregnation method. A suitable concentration of K and Mn promoters for preparation of Co/γ-Al_2O_3 catalysts by solid-state reaction were 1 wt.% for both promoters owing to higher the CO_2 conversion, which giving about 69% and 41%, respectively, when compared to non-promoters catalysts preparation. In case of incipient wetness impregnation (IWI) method that is more interesting. The CO_2 conversion of the addition of 1wt.% K and Mn on Co/γ-Al_2O_3 catalysts were 62% and

15% of non-promoters added Co/γ-Al_2O_3 catalysts since the metals have enhanced cobalt reducibility and significantly improved the surface cobalt metal active site. Therefore, the effect of promoters was more pronounced when the catalysts were prepared by solid-state reaction.

5.2 Recommendations

1. The carbon dioxide hydrogenation reaction was used to produce widely methane under the condition used. It's quite desirable a function of different feed gas ratios of H_2/CO_2, $CO/CO_2/H_2$, operating pressures, as well as reduction temperature.

2. The carbon dioxide, which is feed gas for carbon dioxide hydrogenation reaction, was dissociated to CO and O through mechanism. It's quite interesting to study the mechanism of adsorbed CO_2 by in situ IR analysis.

REFERENCES

[1] Hoekman SK, Broch A, Robbins C, Purcell R. CO_2 recycling by reaction with renewably-generated hydrogen. International Journal of Greenhouse Gas Control. 2010;4(1):44-50.

[2] Joomla. Earth's CO_2 http://co$_2$now.org/2013 [2013, August 13].

[3] Das T, Deo G. Synthesis, characterization and in situ DRIFTS during the CO_2 hydrogenation reaction over supported cobalt catalysts. Journal of Molecular Catalysis A: Chemical. 2011;350(1-2):75-82.

[4] Zhao A, Ying W, Zhang H, Hongfang M, Fang D. Ni/Al_2O_3 catalysts for syngas methanation: Effect of Mn promoter. Journal of Natural Gas Chemistry. 2012;21(2):170-7.

[5] Gnanamani MK, Shafer WD, Sparks DE, Davis BH. Fischer–Tropsch synthesis: Effect of CO_2 containing syngas over Pt promoted Co/γ-Al_2O_3 and K-promoted Fe catalysts. Catalysis Communications. 2011;12(11):936-9.

[6] Das T, Deo G. Promotion of Alumina Supported Cobalt Catalysts by Iron. The Journal of Physical Chemistry C. 2012;116(39):20812-9.

[7] Fischer N, Minnermann M, Baeumer M, Steen E, Claeys M. Metal Support Interactions in Co_3O_4/Al_2O_3 Catalysts Prepared from w/o Microemulsions. Catalysis Letters. 2012;142(7):830-7.

[8] Profeti LPR, Ticianelli EA, Assaf EM. Co/Al_2O_3 catalysts promoted with noble metals for production of hydrogen by methane steam reforming. Fuel. 2008;87(10-11):2076-81.

[9] Wang SL, Wang MK, Tzou YM. Effect of temperatures on formation and transformation of hydrolytic aluminum in aqueous solutions. Colloids and Surfaces A: Physicochemical and Engineering Aspects. 2003;231 (1-3):143-57.

[10] Rozita Y, Brydson R, Scott AJ. An investigation of commercial gamma-Al_2O_3 nanoparticles. Journal of Physics: Conference Series. 2010;241:012096.

[11] Favaro L, Boumaza A, Roy P, Lédion J, Sattonnay G, Brubach JB, et al. Experimental and ab initio infrared study of χ-, κ- and α-aluminas formed from gibbsite. Journal of Solid State Chemistry. 2010;183(4):901-8.

[12] Gary Jacobs, Tapan K. Das, Yongqing Zhang, Jinlin Li, Guillaume Racoillet, Davis BH. Fischer–Tropsch synthesis: support, loading, and promoter effects on the reducibility of cobalt catalysts. Applied Catalysis A: General. 2002;233:263-81.

[13] L. Ji, J. Lin, Zeng HC. Metal-Support Interactions in Co/Al_2O_3 Catalysts: A Comparative Study on Reactivity of Support. J Phys Chem B. 2000;104:1783-90.

[14] Feng Li, Xianghua Yu, Hongjun Pan MW, Xin X. Syntheses of MO_2 (M=Si, Ce, Sn) nanoparticles by solid-state reactions at ambient temperature. Solid State Sciences 2000;2(8):767-72.

[15] Wang W, Wang S, Ma X, Gong J. Recent advances in catalytic hydrogenation of carbon dioxide. Chemical Society reviews. 2011;40(7):3703-27.

[16] Lee S-C, Jang J-H, Lee B-Y, Kim J-S, Kang M, Lee S-B, et al. Promotion of hydrocarbon selectivity in CO_2 hydrogenation by Ru component. Journal of Molecular Catalysis A: Chemical. 2004;210(1-2):131-41.

[17] Park J-N, McFarland EW. A highly dispersed Pd–Mg/SiO_2 catalyst active for methanation of CO2. Journal of Catalysis. 2009;266(1):92-7.

[18] Sang Joon Choe, Hae Jin Kang, Su-Jin Kim, Sung-Bae Park, Dong Ho Park, Huh DS. Adsorbed Carbon Formation and Carbon Hydrogenation for CO_2 Methanation on the Ni(111) Surface: ASED-MO Study. Bull Korean Chem Soc. 2005;26(11):1682-90.

[19] Zhao Y, Wang L, Hao X, Wu J. The kinetic study of light alkene syntheses by CO_2 hydrogenation over Fe-Ni catalysts. Frontiers of Chemical Engineering in China. 2009;4(2):153-62.

[20] Hitoshi Kusama, Kyoko Kitamura Bando, Kiyomi Okabe, Arakawa H. Effect of metal loading on CO_2 hydrogenation reactivity over Rh/SiO2 catalysts. Applied Catalysis A: General 2000;197(2):255-68.

[21] Yu K-P, Yu W-Y, Kuo M-C, Liou Y-C, Chien S-H. Pt/titania-nanotube: A potential catalyst for CO_2 adsorption and hydrogenation. Applied Catalysis B: Environmental. 2008;84(1-2):112-8.

[22] Swalus C, Jacquemin M, Poleunis C, Bertrand P, Ruiz P. CO_2 methanation on Rh/γ-Al_2O_3 catalyst at low temperature: "In situ" supply of hydrogen by Ni/activated carbon catalyst. Applied Catalysis B: Environmental. 2012;125:41-50.

[23] M. Agnelli, M. Kolb, Mirodatos C. Co Hydrogenation on a Nickel Catalyst: 1. Kinetics and Modeling of a Low-Temperature Sintering Process. Journal of Catalysis. 1994;148(1):9-21.

[24] Dorner RW, Hardy DR, Williams FW, Willauer HD. Effects of ceria-doping on a CO_2 hydrogenation iron–manganese catalyst. Catalysis Communications. 2010;11(9):816-9.

[25] Sharma S, Hu Z, Zhang P, McFarland EW, Metiu H. CO_2 methanation on Ru-doped ceria. Journal of Catalysis. 2011;278(2):297-309.

[26] Chu W, Chernavskii P, Gengembre L, Pankina G, Fongarland P, Khodakov A. Cobalt species in promoted cobalt alumina-supported Fischer–Tropsch catalysts. Journal of Catalysis. 2007;252(2):215-30.

[27] Sinkler W, Bradley SA, Ziese U, Jong KPd. 3D-TEM Study of Gamma Alumina Catalyst Supports. Microscopy and Microanalysis. 2006;12(S02):52-3.

[28] Kowalczyk Z, Stołecki K, Raróg-Pilecka W, Miśkiewicz E, Wilczkowska E, Karpiński Z. Supported ruthenium catalysts for selective methanation of carbon oxides at very low CO_x/H_2 ratios. Applied Catalysis A: General. 2008;342(1-2):35-9.

[29] Zhou G, Wu T, Xie H, Zheng X. Effects of structure on the carbon dioxide methanation performance of Co-based catalysts. International Journal of Hydrogen Energy. 2013;38(24):10012-8.

[30] Alphonse P, Courty M. Structure and thermal behavior of nanocrystalline boehmite. Thermochimica Acta. 2005;425(1-2):75-89.

[31] Paglia G. Determination of the Structure of γ-Alumina using Empirical and First Principles Calculations combined with Supporting Experiments: Curtin University of Teachology; 2004.

[32] Barthelmy D. Gibbsite Mineral Data http://webmineral.com/data/Gibbsite.shtml#.UgowqtKU3g3.2013 [2013, August 1].

[33] D.S. MacIver, W.H. Wilmot, Joanne M. Bridges. Catalytic aluminas: II. Catalytic properties of eta and gamma alumina. Journal of Catalysis. 1964;3(3):502–11.

[34] Matori KA, Wah LC, Hashim M, Ismail I, Zaid MH. Phase transformations of alpha-alumina made from waste aluminum via a precipitation technique. International journal of molecular sciences. 2012;13(12):16812-21.

[35] Cava S, Tebcherani SM, Souza IA, Pianaro SA, Paskocimas CA, Longo E, et al. Structural characterization of phase transition of Al2O3 nanopowders obtained by polymeric precursor method. Materials Chemistry and Physics. 2007;103(2-3):394-9.

[36] James H. Kim, Herman J. Gibb, Paul D. Howe. COBALT AND INORGANIC COBALT COMPOUNDS. the United Nations Environment Programme, the International Labour Organization, and the World Health Organization,: Contract No.: 69.

[37] Baek JH, Park JY, Hwang AR, Kang YC. Spectroscopic and Morphological Investigation of Co3O4Microfibers Produced by Electrospinning Process. Bulletin of the Korean Chemical Society. 2012;33(4):1242-6.

[38] Ali S, Mohd Zabidi NA, Subbarao D. Correlation between Fischer-Tropsch catalytic activity and composition of catalysts. Chemistry Central journal. 2011;5:68.

[39] Jacobs G, Ji Y, Davis BH, Cronauer D, Kropf AJ, Marshall CL. Fischer–Tropsch synthesis: Temperature programmed EXAFS/XANES investigation of the influence of support type, cobalt loading, and noble metal promoter

addition to the reduction behavior of cobalt oxide particles. Applied Catalysis A: General. 2007;333(2):177-91.

[40] Jinlin Li, Neil J. Coville. Effect of Pretreatment on Reduction and Activity of the Boron-Modified Co/TiO_2 Fischer-Tropsch Catalyst. Am Chem Soc Div Fuel Chem. 2003;48(2):737.

[41] Trépanier M, Tavasoli A, Anahid S, K. Dalai A. Deactivation Behavior of Carbon Nanotubes Supported Cobalt Catalysts in Fischer-Tropsch Synthesis. iranian j chemistry and chemical engineering. 2011;30(1): 37-47.

[42] Wang H. Kinetic studies of some solid-state reactions of metal sulfides: University of Adelaide; 2005.

[43] Vikas S. Kshirsagar, Subramanian Vijayanand, Hari S. Potdar, Pattayil A. Joy, Kashinath R. Patil, Rode CV. Highly Active Nanostructured Co_3O_4 Catalyst with Tunable Selectivity for Liquid Phase Air Oxidation of p-Cresol. Chemistry Letters. 2008;37(3).

[44] Mu S, Wu Z, Wang Y, Qi S, Yang X, Wu D. Formation and characterization of cobalt oxide layers on polyimide films via surface modification and ion-exchange technique. Thin Solid Films. 2010;518(15):4175-82.

[45] Naruškevičius L, Tamašauskaitė-Tamašiūnaitė L, Žielienė A, Jasulaitienė V. A Co-based surface activator for electroless copper deposition. Surface and Coatings Technology. 2012;206(11-12):2967-71.

[46] Bêche E, Charvin P, Perarnau D, Abanades S, Flamant G. Ce 3d XPS investigation of cerium oxides and mixed cerium oxide ($Ce_xTi_yO_z$). Surface and Interface Analysis. 2008;40(3-4):264-7.

[47] Chun K-Y, Lee CJ. Potassium Doping in the Double-Walled Carbon Nanotubes at Room Temperature. The Journal of Physical Chemistry C. 2008;112:4492-7.

[48] Biesinger MC, Payne BP, Grosvenor AP, Lau LWM, Gerson AR, Smart RSC. Resolving surface chemical states in XPS analysis of first row transition metals, oxides and hydroxides: Cr, Mn, Fe, Co and Ni. Applied Surface Science. 2011;257(7):2717-30.

[49] B.A. Sexton, A.E. Hughes, Turney TW. An XPS and TPR study of the reduction of promoted cobalt-kieselguhr Fischer-Tropsch catalysts. Journal of Catalysis. 1986;97(2):390–406.

[50] DILLARD JG, SCHENCK C, KOPPELMAN M. SURFACE CHEMISTRY OF COBALT IN CALCINED COBALT-KAOLINITE MATERIALS. Clays and Clay Minerals. 1983;31(1):69-72.

[51] Jacobs G, Ribeiro MC, Ma W, Ji Y, Khalid S, Sumodjo PTA, et al. Group 11 (Cu, Ag, Au) promotion of 15%Co/Al_2O_3 Fischer–Tropsch synthesis catalysts. Applied Catalysis A: General. 2009;361(1-2):137-51.

[52] Robert C. Reuel CHB. The stoichiometries of H_2 and CO adsorptions on cobalt: Effects of support and preparation. Journal of Catalysis. 1984;85(63):90110-6.

[53] Diehl F, Khodakov AY. Promotion of Cobalt Fischer-Tropsch Catalysts with Noble Metals: a Review. Oil & Gas Science and Technology - Revue de l'IFP. 2008;64(1):11-24.

[54] Z. Lendzion -Bielun MP, U. Narkiewicz and W. Arabczyk. EFFECT OF STRUCTURAL PROMOTERS ON THE REDUCTION PROCESS OF NANOCRYSTALLINE COBALT OXIDES. Rev.Adv.Mater.Sci. 2006;12:145-9.

[55] Tan BJ, Klabunde KJ, Tanaka T, Kanai H, Yoshida S. An EXAFS study of cobalt-manganese/silica bimetallic solvated metal atom dispersed (SMAD) catalysts1988. 5951-8 p.

APPENDIX

APPENDICES A

CALCULATION FOR CATALYSTS PREPARATION

1. Preparation of the addition second metal in Co/γ-Al_2O_3 catalyst by solid-state reaction.

Preparation of the addition promoters in Co/γ-Al_2O_3 catalyst by solid-state reaction among gibbsite, cobalt nitrate ($Co(NO_3)_2 \cdot 6(H_2O)$), and promoted precursor. The cobalt loading was fixed at 15 wt.%. Several promoters loading (K, Mn, Cu, and Ce) were prepared: 0.0, 0.5, 1.0, and 2.0 wt.%. Thereby, the catalysts preparation is shown as follows:

- Preparation of the 1MnCo/γ-Al_2O_3 catalyst using promoted manganese acetate ($Mn(C_2H_3O_2)_2 \cdot 6(H_2O)$). It's fixed 1.0 wt.% of Mn and 15 wt.% of Co which can be displayed as follows :

Reactant

Molecular weight

- Gibbsite ($Al(OH)_3$) : 78 g/mole
- Cobalt nitrate ($Co(NO_3)_2 \cdot 6(H_2O)$) : 291.03 g/mole
- Manganese acetate ($Mn(C_2H_3O_2)_2 \cdot 6(H_2O)$) : 245.90 g/mole

Calculation

For preparation 100 g of 1MnCo/γ-Al_2O_3 catalyst, which fixed 1.0 wt.% of Mn and 15 wt.% of Co. This catalyst consists of cobalt (Co), manganese (Mn) metal, and gamma alumina (γ-Al_2O_3) and can be calculated as follows:

Co	=	15	g		
Mn	=	1	g		
γ-Al_2O_3	=	100 - (15 + 1)		=	84

A desirable amount of cobalt metal is equal to 15 g prepared from cobalt nitrate ($Co(NO_3)_2{\cdot}6(H_2O)$) precursor which has molecular weight as 291.03 g/mole and molecular weight of cobalt as 56.93 g. Thus, the catalyst can be calculated as follows:

$Co(NO_3)_2{\cdot}6(H_2O)$ $$= 15\ g\ Co \times \frac{291.03\ g\ Co(NO_3)_2 \cdot 6(H_2O)}{56.93\ g\ Co}$$

$$= 76.68\ g$$

For promoted manganese which is prepared from manganese acetate ($Mn(C_2H_3O_2)_2{\cdot}6(H_2O)$) is required 1 g. Molecular weight of manganese as 54.94 g

$Mn(C_2H_3O_2)_2{\cdot}6(H_2O)$ $$= 1\ g\ Mn \times \frac{245.90\ g\ Mn(C_2H_3O_2)_2 \cdot (H_2O)}{54.94\ g\ Mn}$$

= 4.26 g

The Al_2O_3 which is support was transformed to role in calcination gibbsite ($Al(OH)_3$). Accordingly, 84 g of □-Al_2O_3 which was prepared from gibbsite can be calculated as follows:

($Al(OH)_3$) $$= 84\ g\ Al_2O_3 \times \frac{2 \times 26.98\ g\ Al}{84.96\ g\ Al_2O_3} \times \frac{78\ g\ Al(OH)_3}{26.98\ g\ Al}$$

= 152.44 g

In the same amount of promoters (1 wt.%) which were prepared by solid-state reaction such as potassium, cupper, and cerium. Those catalysts can be calculated with the same method. The precursors of promoters were followers:

- Potassium nitrate KNO_3

  Molecular weight: 101.1 g/mole

- Cupper nitrate $(Cu(NO_3)_2)\cdot 3H_2O$

  Molecular weight: 241.6 g/mole

- Cerium acetate $(Ce(C_2H_3O_2))\cdot xH_2O$

  Molecular weight: 317.26 g/mole

➢ Preparation of the addition promoters in Co/γ-Al_2O_3 catalyst by solid-state reaction among gibbsite, cobalt nitrate $(Co(NO_3)_2\cdot 6(H_2O))$, and promoted precursor with mole ratio of Co/Al and X/Co (X = K, Mn, Cu, and Ce) equal to 1/5 and 0.7, respectively. Thereby, the catalysts preparation is shown as follows:

Calculation

For 1MnCo/γ-Al_2O_3 catalyst using promoted manganese acetate $(Mn(C_2H_3O_2)_2\cdot 6(H_2O))$. It's fixed mole ratio of Co/Al and X/Co (X = K, Mn, Cu, and Ce) equal to 1/5 and 0.7, respectively. It can be displayed as follows:

Reactant

Molecular weight

- Gibbsite $(Al(OH)_3)$: 78 g/mole
- Cobalt nitrate $(Co(NO_3)_2\cdot 6(H_2O))$: 291.03 g/mole
- Manganese acetate $(Mn(C_2H_3O_2)_2\cdot 6(H_2O))$: 245.90 g/mole

Calculation

For preparation 100 g of gibbsite can be calculated as follows:

Aluminum $= 100\ g\ Al(OH)_3 \times \frac{1\ mole\ Al(OH)_3}{78\ g\ Al(OH)_3} \times \frac{1\ mole\ Al}{1\ mole\ Al(OH)_3} \times \frac{26.98\ g\ Al}{1\ mole\ Al}$

= 34.59 g Al

$= 34.59\ g\ Al \times \frac{1\ mole\ Al}{26.98\ g\ Al}$

= 1.28 mole Al

For mole ratio of Co/Al = 1/5

Co required $= 1.28\ mole\ Al \times \frac{1\ mole\ Co}{5\ mole\ Al}$

= 0.27 mole Co

$= 0.27\ mole\ Co \times \frac{58.93\ g\ Co}{1\ mole\ Co}$

= 15.08 g Co

A desirable amount of cobalt metal is equal to 15.08 g prepared from cobalt nitrate ($Co(NO_3)_2 \bullet 6(H_2O)$) precursor which has molecular weight as 291.03 g/mole and molecular weight of cobalt as 56.93 g. Thus, the catalyst can be calculated as follows:

$Co(NO_3)_2 \cdot 6(H_2O)$ $= 15\ g\ Co \times \frac{291.03\ g\ Co(NO_3)_2 \cdot 6(H_2O)}{56.93\ g\ Co}$

$= 76.68\ g$

For mole ratio of Mn/Co = 0.7

Mn required $= 0.27\ mole\ Co \times \frac{0.7\ mole\ Mn}{1\ mole\ Co}$

= 0.19 mole Mn

$= 0.19\ mole\ Mn \times \frac{54.94\ g\ Mn}{1\ mole\ Mn}$

= 10.44 g Mn

For promoted manganese which is prepared from manganese acetate ($Mn(C_2H_3O_2)_2 \cdot 6(H_2O)$) is required 10.44 g. Molecular weight of manganese (Mn) as 54.94 g

$Mn(C_2H_3O_2)_2 \cdot 6(H_2O)$ $= 10.44\ g\ Mn \times \frac{245.90\ g\ Mn(C_2H_3O_2)_2 \cdot (H_2O)}{54.94\ g\ Mn}$

= 46.73 g

The Al_2O_3 which is support was transformed to role in calcination gibbsite ($Al(OH)_3$). Accordingly, 84 g of γ-Al_2O_3 which was prepared from gibbsite can be calculated as follows:

$(Al(OH)_3)$ $= 84\ g\ Al_2O_3 \times \frac{2 \times 26.98\ g\ Al}{84.96\ g\ Al_2O_3} \times \frac{78\ g\ Al(OH)_3}{26.98\ g\ Al}$

= 152.44 g

In the same amount of promoters (1 wt.%) which were prepared by solid-state reaction such as potassium, cupper, cerium. The precursors of promoters were followers:

- Potassium nitrate (KNO_3)

Molecular weight: 101.1 g/mole

- Cupper nitrate (($Cu(NO_3)_2$).$3H_2O$)

Molecular weight: 241.6 g/mole

- Cerium acetate (($Ce(C_2H_3O_2)$).xH_2O)

Molecular weight: 317.26 g/mole

2. Preparation of the addition second metal in Co/γ-Al_2O_3 catalyst by incipient wetness impregnation method.

Formerly, the addition second metal in Co/γ-Al_2O_3 catalysts were prepared by solid-state reaction which add with 1 wt.% of promoters. Thereby, the composition of catalysts, which were prepared by incipient wetness impregnation method, is shown as follows:

➢ Preparation of the 1MnCo/γ-Al_2O_3 catalyst using promoted manganese acetate ($Mn(C_2H_3O_2)_2{\cdot}6(H_2O)$). It's fixed 1.0 wt.% of Mn and 15 wt.% of Co which can be displayed as follows :

Reactant

Molecular weight

- Gibbsite ($Al(OH)_3$) : 78 g/mole
- Cobalt nitrate ($Co(NO_3)_2{\cdot}6(H_2O)$) : 291.03 g/mole
- Manganese acetate ($Mn(C_2H_3O_2)_2{\cdot}6(H_2O)$) : 245.90 g/mole

Calculation

For preparation 100 g of 1MnCo/γ-Al_2O_3 catalyst, which fixed 1.0 wt.% of Mn and 15 wt.% of Co. This catalyst consists of cobalt (Co), manganese (Mn) metal, and gamma alumina (γ-Al_2O_3) and can be calculated as follows:

Co = 15 g

Mn = 1 g

γ-Al_2O_3 = 100-(15 + 1) = 84 g

A desirable amount of gamma-alumina (γ-Al_2O_3) is equal to 84 g from the calcined gibbsite ($Al(OH)_3$) precursor at 650 °C for 5 h. which has molecular weight as 78 g/mole and molecular weight of aluminum (Al) as 26.98 g.

A desirable amount of cobalt metal is equal to 15 g prepared from cobalt nitrate ($Co(NO_3)_2{\cdot}6(H_2O)$) precursor which has molecular weight as 291.03 g/mole and molecular weight of cobalt as 56.93 g. Thus, the catalyst can be calculated as follows:

$$Co(NO_3)_2{\cdot}6(H_2O) = 15\ g\ Co \times \frac{291.03\ g\ Co(NO_3)_2 \cdot 6(H_2O)}{56.93\ g\ Co}$$

$$= 76.68\ g$$

For promoted manganese which is prepared from manganese acetate ($Mn(C_2H_3O_2)_2{\cdot}6(H_2O)$) is required 1 g. Molecular weight of manganese as 54.94 g

$$Mn(C_2H_3O_2)_2{\cdot}6(H_2O) = 1\ g\ Mn \times \frac{245.90\ g\ Mn(C_2H_3O_2)_2 \cdot (H_2O)}{54.94\ g\ Mn}$$

= 4.26 g

In the same amount of another promoter which were prepared by incipient wetness impregnation method. Another precursor of K promoted was followers:

- Potassium nitrate (KNO_3)

Molecular weight: 101.1 g/mole

APPENDICES B

CALIBRATION CURVES

The calibration curve was used to calculate for composition of reactants and products in CO_2 hydrogenation. The reactants consist of CO_2 and H_2. For the main gaseous product is methane; moreover, CO is a by-product. The gaseous products and reactants were analyzed by a gas chromatograph (Shimadzu GC-8A) equipped with a thermal conductivity detector (TCD), a molecular sieve column for H_2, CO, CH_4 and a polapak-Q column for CO_2 separation.

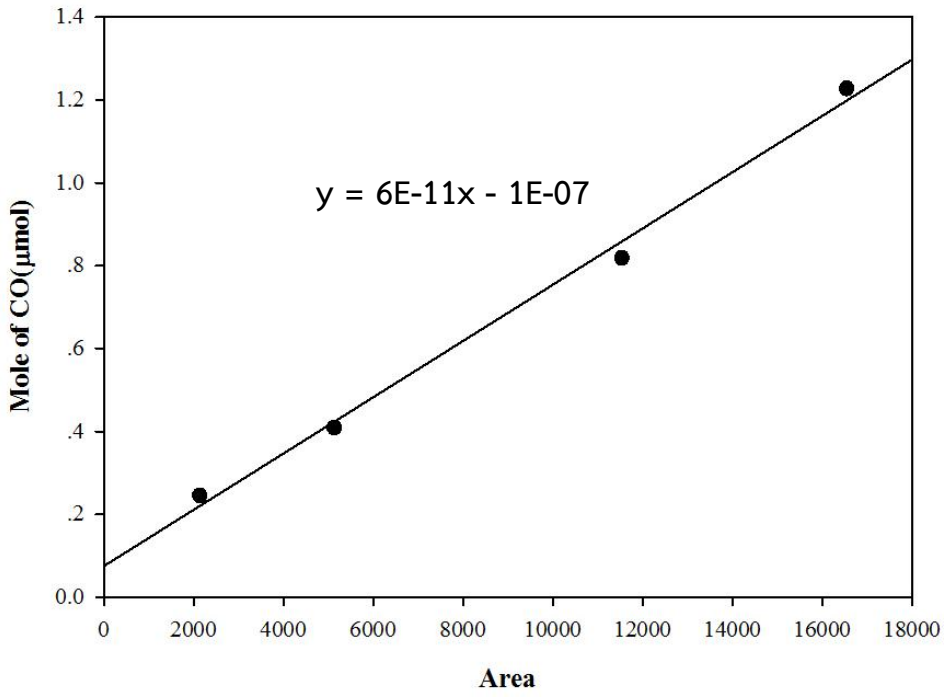

Figure B.1 Calibration curve of CO

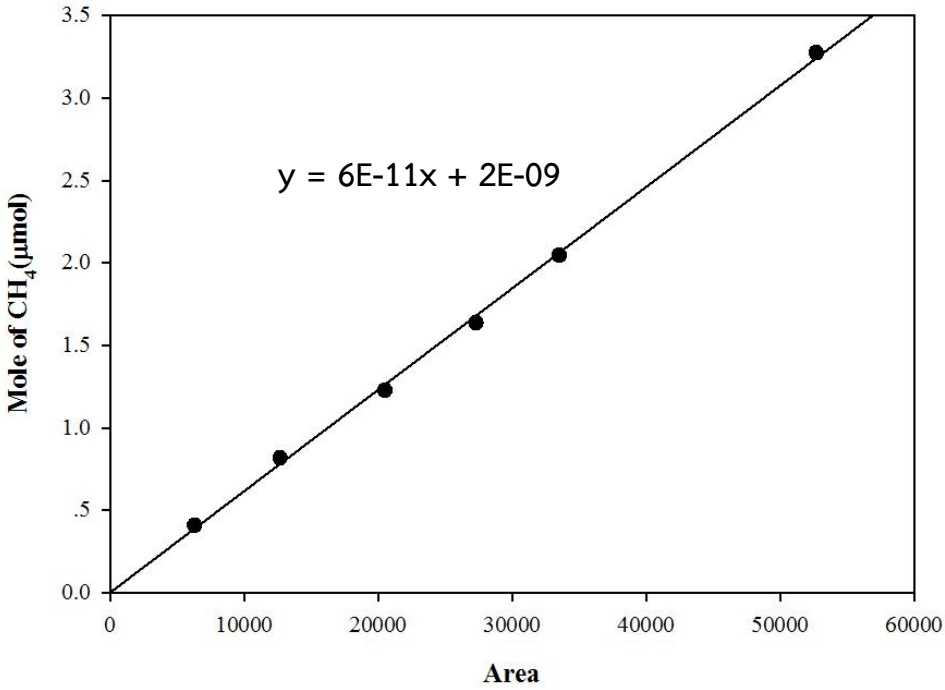

Figure B.2 Calibration curve of CH_4

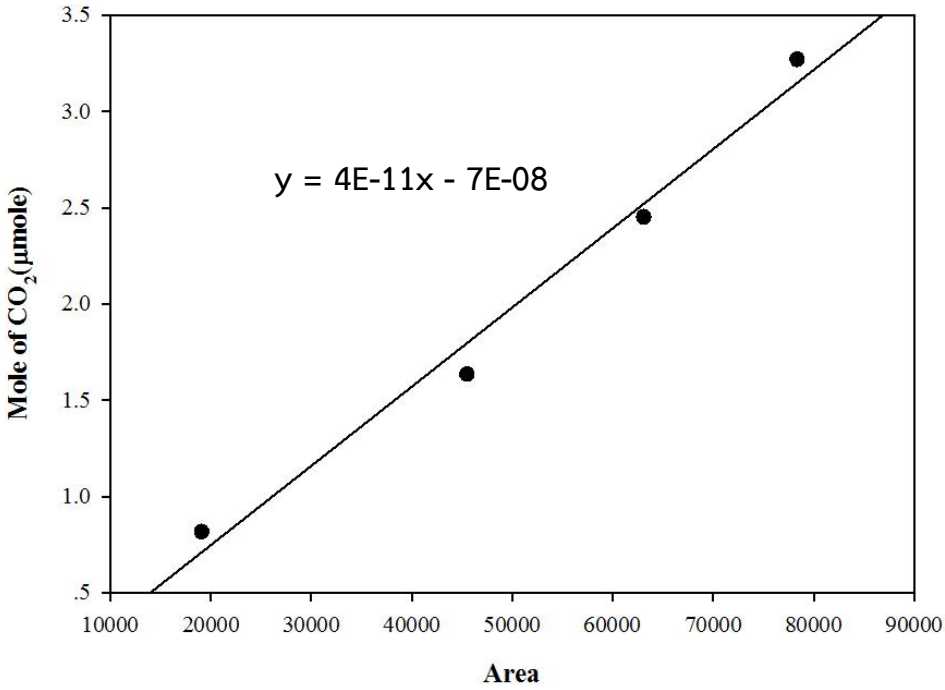

Figure B.3 Calibration curve of CO_2

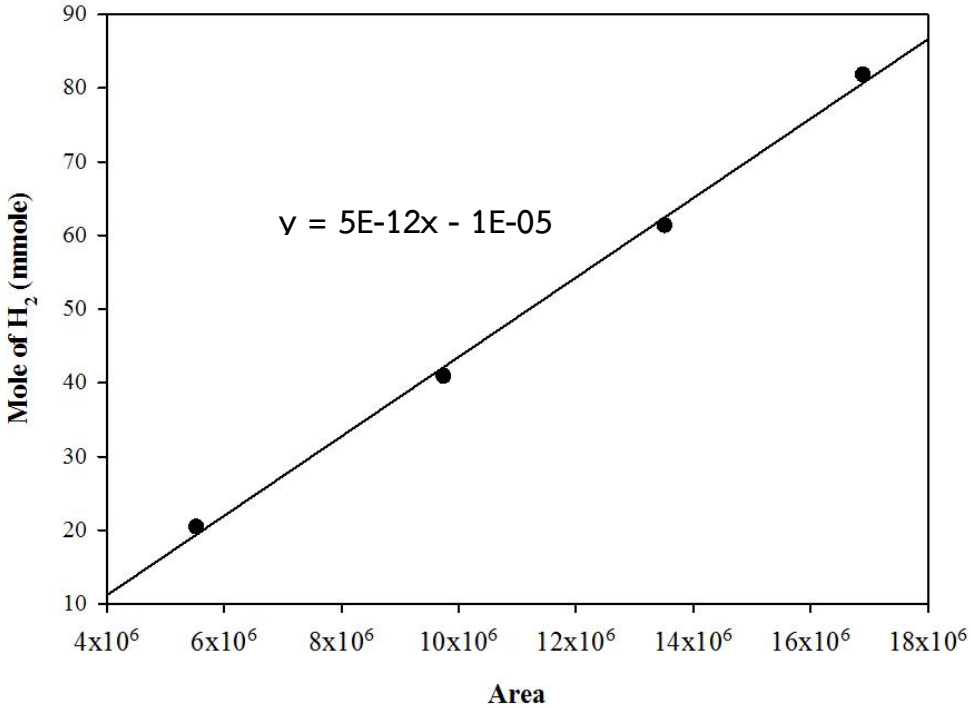

Figure B.4 Calibration curve of H_2

APPENDICES C

CALCULATION FOR CO_2 CONVERSION AND CH_4 FORMATION

The catalysts performance was evaluated with the CO_2 conversion and CH_4 formation, the gaseous product and reactant were analyzed after steady-state operation under condition.

The gaseous products and reactants were analyzed by a gas chromatograph (Shimadzu GC-8A). CO_2 conversion is evaluated with mole of CO_2 which converted with calibration curve of CO_2. Therefore, CO_2 conversion was defined as follows:

$$CO_2\ conversion = \frac{mole\ of\ CO_2\ in\ feed - mole\ of\ CO_2\ in\ product}{mole\ of\ CO_2\ in\ feed} \times 100$$

Reaction rate was estimated from CO_2 conversion as follows:

Weight of catalysts used	=	W	g
Flow rate of CO_2	=	2	cc/min
Reaction time	=	60	min
Weight of CH_2	=	14	g
Volume of 1 mole of gas at 1atm	=	22400	cc

$$\text{Reaction rate}\ (g\ CH_2 / g\ of\ catalysts.h) = \frac{\left(\frac{\%\ CO_2\ conversion}{100}\right) \times 60 \times 14 \times 2}{W \times 22400}$$

APPENDICES D

CALCULATION FOR CRYTALLITE SIZE

Calculation for the crystallite size of Co_3O_4 with Scherrer equation

The average crystallites size of Co_3O_4 can be calculated by the half-height width of diffraction peak from XRD pattern by using the Scherer equation:

$$D = \frac{K\lambda}{\beta \cos\theta} \qquad \text{(D.1)}$$

Where D : Crystallite size, Å

K : Sharp factor or the Scherrer constant = 0.9

λ : Wavelength of the x-ray, 1.54056 Å for CuK_α

β : The full-width-half-max (FWHM) of the peak after correcting for peak broadening, which is caused by the diffractometer, radian

θ : Bragg angle, radian

The full-width-half-max (FWHM) of the peak after correcting for peak broadening (β) can be obtained by using Warren's equation:

$$\beta^2 = \beta_M^2 - \beta_S^2 \qquad \text{(D.2)}$$

So,

$$\beta = \sqrt{\beta_M^2 - \beta_S^2}$$

Where B_S: The FWHM of a standard material, which is α- Al_2O_3

B_M: The FWHM of peak broadening due to the machine

Example: Calculation for the crystallite size of Co_3O_4 for Co/γ-Al_2O_3

The FWHM of peak (β_M) at 2θ value of 37° = 0.226196°

$$= \frac{2\pi \times 0.226196}{360} \text{ radian}$$

= 0.00395 radian

The equation is shown in **Figure D.1.** It can calculate β_S at 2θ value of 37°

So, the FWHM of α- Al_2O_3 (β_S) = 0.0008147

So, $$\beta = \sqrt{0.00395^2 - 0.0008147^2}$$

β = 0.00386

2θ = 37°

θ = 18.5°

= 0.3229 radian

λ = 1.54056 Å

$$The\ crystallite\ size = \frac{0.9 \times 1.54056}{0.00386 \times \cos(0.3229)} = 378.49 \text{ angstronm} = 37.8 \text{ nm}$$

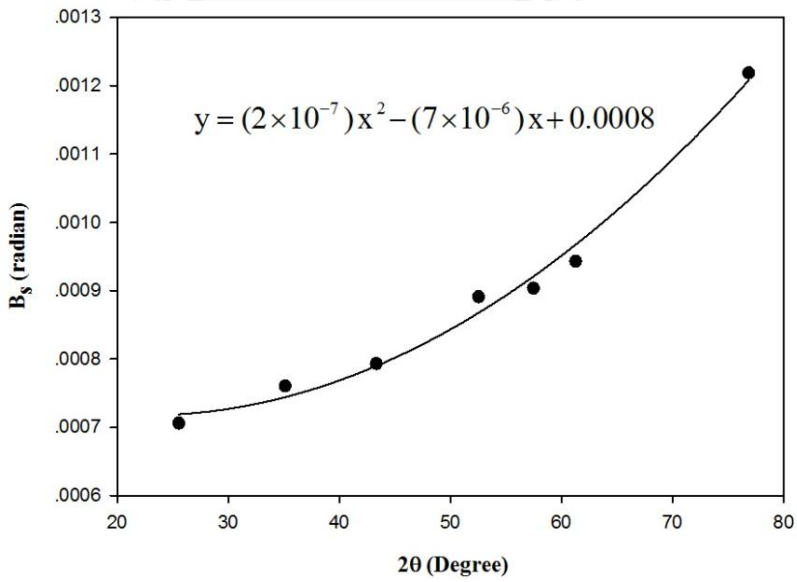

Figure D.1 Plot of the peak widths (FWHM) for α-Al_2O_3 at various diffraction angles

APPENDICES E

CALCULATION FOR REDUCIBILITY

The area of peaks during TPR can be obtained based on 0.1 g of the catalysts sample. The Ag_2O sample was used to be the calibration for calculation of H_2 consumption with Co_3O_4. For alumina supported cobalt catalysts, it can be assumed that the major species of Co, which was reduced, is Co_3O_4. From ICP analysis, the actual amount of cobalt for both solid-state reaction and incipient wetness impregnation method was 10 wt.% and 13 wt.%, respectively. Therefore, the amount of H_2 consumption by Co_3O_4 is calculated as follow:

Reactant

Molecular weight of Ag_2O: 231.73 g/mole

Molecular weight of Ag: 107.86 g/mole

Molecular weight of Co: 58.93 g/mole

Molecular weight of Co_3O_4: 240.79 g/mole

Based on 0.1 g of Ag_2O

Equation of Ag_2O reduction: $Ag_2O + H_2 \rightarrow 2Ag + H_2O$

The weight of Ag_2O used = 0.1 g

$$= \frac{0.1\, g\ Ag_2O}{231.73\, g/mole\ Ag_2O}$$

$= 4.3 \times 10^{-4}$ mole Ag_2O

From equation of Co_3O_4 reduction shows mole ratio of H_2/Co_3O_4 = 1:1.

Thus, H_2 consumption at 100% reducibility = mole of Ag_2O

= 4.3×10^{-4} mole

= 430 μmole

So, the amount of H_2 for the Ag_2O sample is 430 μmole related to the integral area during TPR of Ag_2O sample after reduction 101.95 units

Calculation of reducibility of cobalt catalyst

$$\%reducibility = \frac{Amount\ of\ H_2\ consume\ to\ reduce\ 0.1\ g\ of\ the\ catalyst}{Amount\ of\ theortical\ H_2 consume\ to\ Co_3O_4\ to\ Co^0 of\ 1\ g\ catalyst} \times 100$$

The weight of the cobalt catalyst = W g

The actual amount of cobalt catalyst = Y%

The weight of Co^0 of the cobalt catalyst = $W \times \frac{Y}{100}$

Mole of Co_3O_4 of the cobalt catalyst

$$= W \times \frac{Y}{100} \times \frac{240.79\ g/mole\ Co_3O_4}{(3 \times 58.93) g\ of\ Co/mole Co_3O_4} \times \frac{1\ mole\ Co_3O_4}{240.79\ g/mole\ Co_3O_4}$$

$$= W \times \frac{Y}{100} \times \frac{1}{(3 \times 58.93)} \quad \text{mole}$$

From equation of Co_3O_4 reduction shows mole ratio of H_2/Co_3O_4 = 4:1

The amount of H_2 consumption theoretical = $4 \times mole\ of\ Co_3O_4$

Integral area during TPR of the catalyst = X unit

The actual amount of H_2 consumption = $\frac{430 \times X}{101.95}$ μmole

Calculation of the H_2 consumption of cobalt oxide (Co_3O_4) follow the

Based on 0.1 g of Co/γ-Al_2O_3 prepared by solid-state reaction had 10 wt.%, which was indicated by ICP analysis.

Equation of Co_3O_4 reduction: $Co_3O_4 + 4H_2 \rightarrow 3Co + 4H_2O$

The weight of Co/γ-Al_2O_3 = 0.1 g

Mole of Co_3O_4 of the cobalt catalyst = $0.1 \times \frac{10}{100} \times \frac{1}{(3 \times 58.93)}$

= 5.66×10^{-5} mole Co_3O_4

From equation of Co_3O_4 reduction shows mole ratio of H_2/Co_3O_4 = 4:1.

Thus, H_2 consumption at 100% reducibility = 4 × mole of Co_3O_4

= $4 \times (5.66 \times 10^{-5})$ mole

= 2.26×10^{-4} mole

= 226 μmole

Thus, the amount of H_2 for the Co catalyst prepared by solid-state reaction that can be consumed at 100% reducibility is 2.26 μmole.

Note: for Co catalyst prepared by incipient wetness impregnation, using the same method, it is found that it can consume 294 μmole of H_2 (at 100% reducibility).

Example for 1KCo/γ-Al_2O_3 catalyst prepared by solid-state reaction

Integral area during TPR of the 1KCo/γ-Al_2O_3 catalyst = 45.94 unit

The weight of the 1KCo/γ-Al_2O_3 catalyst = 0.1 g

The actual amount of H_2 consumption $= \frac{430 \times 45.94}{101.95}$ μmole

= 193.76 μmole

$$\%reducibility = \frac{193.76\ \mu mole}{226\ \mu mole} \times 100$$

$$= 86\%$$

APPENDICES F

CALCULATION FOR HYDROGEN CHEMISORPTION

To calculate H_2 uptake, cobalt dispersion, and Co^0 crystallite size, which a stoichiometry of H/Co = 1/2, was measured by H_2 chemisorption as follows:

Let the weight of catalysts	=	W	g	
%Metal loading	=	M		
Molecules weight of metal	=	A	g/mole	
Stoichiometry factor	=	S_f	=	2
Integral area of 100 μl of H_2 peak	=	X	unit	
Integral area of H_2 peak after adsorption	=	Y_i	unit	

Amount of H_2 adsorbed on catalyst = $\sum(X - Y_i)$ unit

Volume of H_2 adsorbed on catalyst = $100 \times \left[\frac{\sum(X - Y_i)}{X}\right]$ μl

Volume of 1 mole of H_2 = V_g μl

Mole of H_2 adsorbed on catalyst

$$= \left[\frac{100}{V_g}\right] \times \left[\frac{\sum(X - Y_i)}{X}\right] \quad \mu\text{mole}$$

Molecule of H_2 adsorbed on catalyst

$$= \left[\frac{100}{V_g}\right] \times \left[\frac{\sum(X - Y_i)}{X}\right] \times \left(6.02 \times 10^{23}\right) \text{ molecule } H_2$$

Total H_2 chemisorption (Metal active site)

$$= \left[\frac{S_f}{W}\right] \times \left[\frac{100}{V_g}\right] \times \left[\frac{\sum(X - Y_i)}{X}\right] \times \left(6.02 \times 10^{23}\right) \text{ molecule } H_2/\text{g cat.}$$

Molecules of Co loaded $= \dfrac{W \times \left(\dfrac{M}{100}\right)}{A} \times \left(6.02 \times 10^{23}\right)$

Calculation of %metal dispersion

$$\%Dispersion = \frac{\text{Metal active site}}{\text{No. molecules of Co loaded}} \times 100 \qquad \text{(F.1)}$$

$$\text{Crystallite size metal} = \frac{99.65}{\%dispersion} \qquad \text{(F.2)}$$

VITA

Miss Mintra sungsook was born 0n 17th December 1989, in Phetchaburi, Thailand. She acknowledged Bachelor degree of from Chulalongkorn University, Thailand in 2012. Since 2012, She had been studying Master degree of Engineering which is department of Chemical Engineering, Chulalongkorn University.

List of publication:

Mintra sungsook, and Joongjai Panprenot, “Effect of K, Mn, Cu, and Ce promoters on the performance of Co/Al2O3 catalysts in CO2 hydrogenation”, The 3rdTIChE International Conference 2013, Khon Kean, Thailand, October 17-18, 2013.